ISSN: 2614-8757 (Print) 2615-2347 (Online)

CHEESA

CHEMICAL ENGINEERING RESEARCH ARTICLES

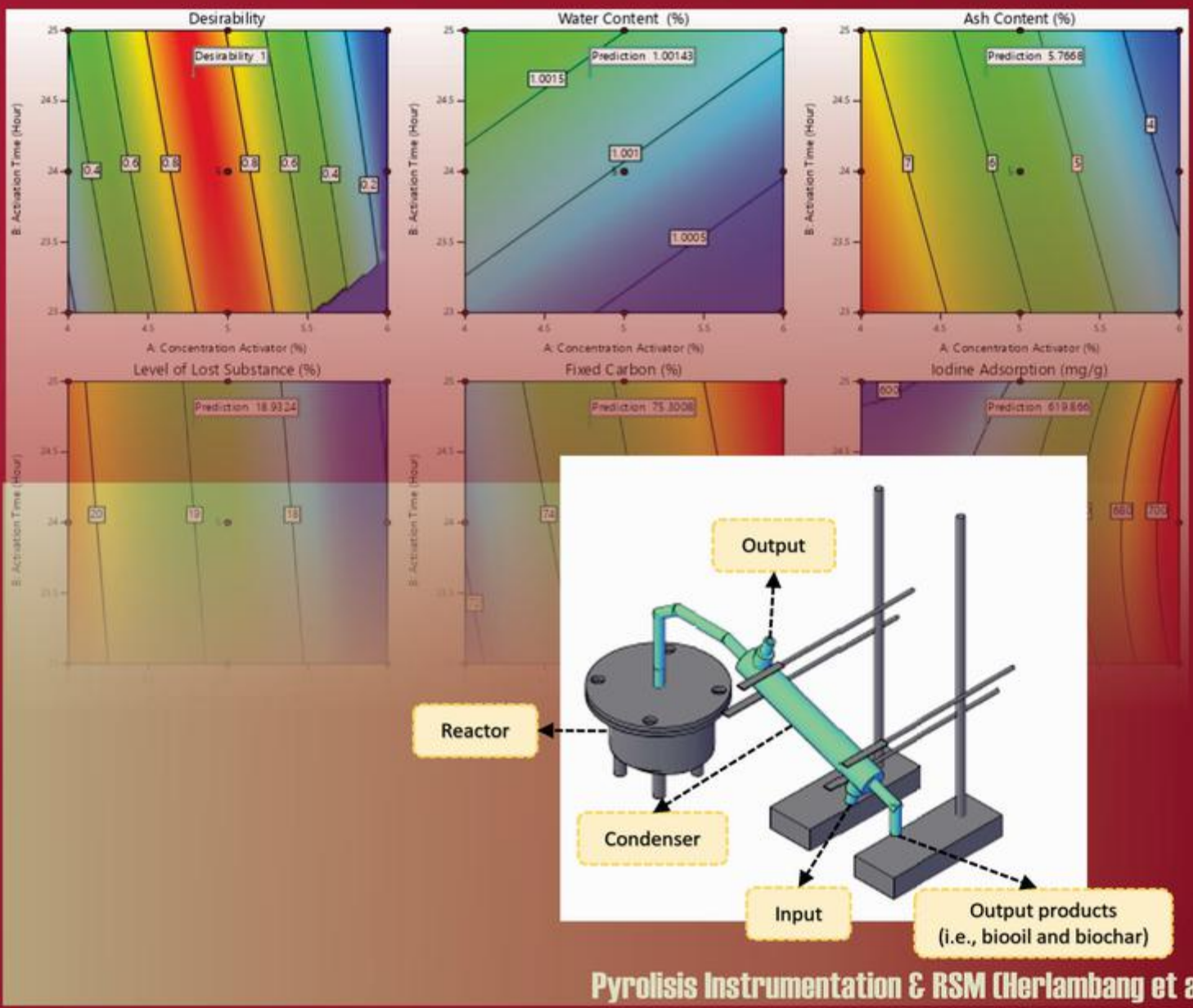

Pyrolisis Instrumentation & RSM (Herlambang et al)

sinta Science and Technology Index DOAJ

VOLUME 6 NO 2, DECEMBER 2023

EDITORIAL BOARD

CHEESA: Chemical Engineering Research Articles

Volume 6 No 2, 2023
ISSN 2614-8757 (Print), ISSN 2615-2347 (Online)
Available online at: http://e-journal.unipma.ac.id/index.php/cheesa

Volume 6 No 2, 2023
ISSN 2614-8757 (Print), ISSN 2615-2347 (Online)
Available online at: http://e-journal.unipma.ac.id/index.php/cheesa

ACKNOWLEDGMENT

CHEESA: Chemical Engineering Research Articles

Our highest gratitude and appreciation go to the reviewers who have reviewed the submitted manuscripts and provided suggestions to us. The reviewers who contributed to this issue are,

1. Prof. Johnner P. Sitompul, Ph.D
2. Prof. Mery Napitupulu, Ph.D
3. Prof. Husni Husin
4. Prof. Dr. Poedji Loekitowati Hariani
5. Dr. Eng. Dewi Agustina Iryani
6. Dr. Anthoni Batahan Aritonang
7. Dr. Rhenny Ratnawati
8. Dr. Safrina Hapsari
9. Dr. Haqqyana
10. Dr. Zuhdi Ma'sum
11. Erni Misran, Ph.D
12. Wahyu Prasetyo Utomo
13. Said Ali Akbar
14. Rokiy Alfanaar
15. Cucuk Lusiani

with the seriousness and thoroughness of the reviewers, help us to improve a quality and maintain the quality of writing in the CHEESA: Chemical Engineering Research Articles Volume 6 No 2, December 2023.

Our thanks also go to the various parties who have helped, so that this edition can be published online according to the specified time.

Editorial
CHEESA

ISSN 2614-8757 (Print), ISSN 2615-2347 (Online)
Available online at: http://e-journal.unipma.ac.id/index.php/cheesa

TABLE OF CONTENTS

CHEESA: Chemical Engineering Research Articles

CHEESA is a journal that becomes a media of study for chemical and chemical engineering. This journal serves as a media for publication of research in chemistry and chemical engineering aimed at academics, practitioners and community at large. Articles that were published in the CHEESA Journal have gone through editing according to established rules without changing the original manuscript.

Volume 6 No 2, 2023

ISSN 2614-8757 (Print), ISSN 2615-2347 (Online) Available online at: http://e-journal.unipma.ac.id/index.php/cheesa

CHEESA: Chemical Engineering Research Articles
ISSN **2614-8757 (Print)**, ISSN **2615-2347 (Online)**
Available online at: http://e-journal.unipma.ac.id/index.php/cheesa

Research Article

Catalyst Lifetime Analysis for High-Temperature Shift Converter (104-D1) at Urea Factory

Analisis Katalis Lifetime pada High-Temperature Shift Converter (104-D1) di Pabrik Urea

Rahmatullah[1*)], Rizka Wulandari Putri[1)], Bobi Mahendra[1)], Hegar Tifal Arofi[1)], Cecep Sumiratna Hadi[2)]

[1)]Universitas Sriwijaya, Chemical Engineering Department, Indonesia
[2)]PT. Pupuk Sriwidjaja Palembang, Indonesia

Article History
Received: 21th Maret 2023; Revised: 08th November 2023; Accepted: 08th November 2023;
Available online: 21th November 2023; Published Regularly: December 2023

doi: 10.25273/cheesa.v6i2.15986.76-84
*Corresponding Author.
Email: rahmatullah@ft.unsri.ac.id

Abstract

The High-Temperature Shift Converter (HTSC) (104-D1) is crucial for converting CO gas into CO_2 in the ammonia unit. This is vital as the presence of CO poses a potential threat to the catalyst in the ammonia converter. In addition, maintaining HTSC (104-D1) at optimal performance is crucial, and this is achieved when the percentage of CO outlet remains below 3.41 mol% on a dry basis. The performance of HTSC (104-D1) was influenced by operating conditions (pressure and temperature) and the ratio of steam to carbon. The increase in temperature leads to an increase in the reaction rate and a decrease in CO conversion due to a decrease in catalyst performance. Therefore, this research aimed to assess the performance of HTSC (104-D1) after the Turn-Around process, specifically focusing on the CO conversion results and operating conditions. The analysis compared actual HTSC temperature, pressure drop, and CO conversion with design data using regression equations. This method predicted a catalyst lifetime of approximately 4 years and 8 months post-Turn-Around.

Keywords: Catalyst lifetime; CO conversion; shift converter; Turn Around

Abstrak

High-Temperature Shift Converter (HTSC) 104-D1 memiliki fungsi untuk mengonversi gas CO menjadi CO_2 pada unit ammonia. Keberadaan CO dapat menjadi racun bagi katalis di ammonia converter. Performa HTSC (104-D1) dikatakan baik apabila persen CO outlet dibawah 3,41 mol% dry basis. Kinerja HTSC (104-D1) dipengaruhi oleh kondisi operasi (tekanan dan temperature) serta rasio steam to carbon. Peningkatan temperature di HTSC (104-D1) menyebabkan naiknya laju reaksi dan turunnya konversi CO karena kinerja katalis yang menurun. Penelitian bertujuan untuk mengetahui bagaimana kinerja dari HTSC (104-D1) setelah Turn Around (Penggantian katalis) berdasarkan kondisi operasi dan konversi CO. Analisa dilakukan dengan membandingkan suhu, penurunan tekanan, dan konversi CO dari data aktual dengan data desain menggunakan metode persamaan regresi untuk memprediksi lifetime katalis. Lifetime katalis HTSC diperkirakan dapat dipakai sampai dengan 4 tahun 8 bulan setelah Turn Around.

***Kata kunci**: Konversi CO; lifetime katalis; shift converter; Turn Around*

1. Introduction

The fertilizer business is a crucial strategic sector for enhancing a nation's economy by playing an important role in supporting increased agricultural production. Urea fertilizer is widely used in agriculture, and is a key product of PT. Pupuk Sriwidjaja Palembang is an Indonesian fertilizer industry offering a range of products including urea, NPK, and ammonia fertilizers.

Ammonia is generated through the reaction of nitrogen gas from the air and hydrogen derived from natural gas [1]. As a crucial raw material in urea production at PT. Pupuk Sriwidjaja, ammonia undergoes a multi-unit production process, namely feed treating units, reforming units, purification & methanation, as well as compression synlopp & refrigeration units [2]. The ammonia produced is then used as a raw material in the urea manufacturing process through its reaction with carbon dioxide (CO_2). The synthesis gas (syngas), which consists of a mixture of hydrogen and nitrogen gases, has a major effect on the production of ammonia. The production of synthetic gas occurs in two stages, namely in primary and secondary reforming, yielding hydrogen, CO, and CO_2 [3].

The synthesis gas purification process consists of three main parts. First, the conversion of CO into CO_2 in the shift conversion unit, second, the absorption of CO_2 by Benfield's solution in the CO_2 absorber. The third stage is the conversion of CO and CO_2 gas into methane gas in the methanator process unit. To optimize hydrogen yield and remove CO, synthesis gas will be supplied to the shift converter [4], where CO reacts with steam (H_2O) to form CO_2 and hydrogen in an exothermic and reversible process, as shown in the following reaction.

$$CO_{(g)} + H_2O_{(v)} \rightleftharpoons CO_{2(g)} + H_{2(g)}$$

In the shift converter, the reactions are both exothermic and reversible [5]. According to the Arrhenius law, increasing the temperature accelerates the rate of reaction [6]. However, in line with the Le Chatelier principle (thermodynamics), a temperature decrease shifts the equilibrium to the right [7]. Favorable thermodynamic conditions, promoting CO conversion and high hydrogen yield, result from exothermic reactions [8]. The shift conversion reaction in industry is operated in two stages, including at high and low temperature.

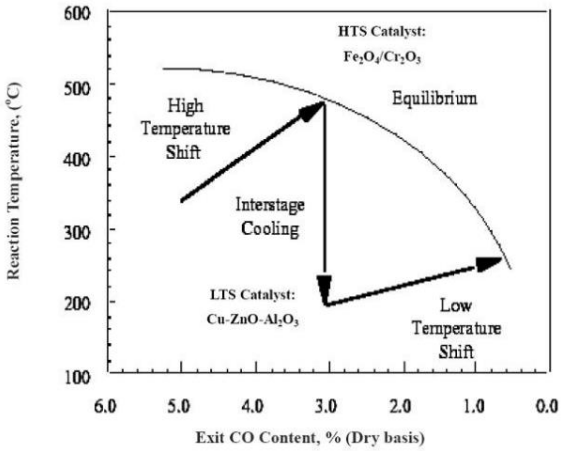

Figure 1. Water gas shift reaction scheme [9]

Figure 1 shows the relationship between the reaction temperature and the percentage of unreacted CO, where in the High-Temperature Shift Converter (HTSC) the percentage of unreacted CO is around 3%. Subsequently, CO conversion is relatively low when the operating temperature deviates significantly from the equilibrium temperature. Raising the temperature is required to improve conversion and quicken the rate of reaction. The concentration of CO

decreases in the reactor due to the greater temperature, while the concentration of H_2 and CO_2 increases. CO_2 and H_2 concentrations will rise until the reactor achieves its maximum temperature, however, excessive temperature increases will lead the reduction in the composition of CO_2 and H_2. This happens as the reaction reaches equilibrium, shifting to the left and raising the CO concentration.[10].

CO in the process gas is undesirable due to its toxicity in catalyst of ammonia converter, necessitating purification from the process [11]. This includes shift conversion of CO to CO_2 followed by re-converted in the methanator. Shift conversion to CO occurs in HTSC and Low-Temperature Shift Converter (LTSC) within the ammonia plant. Inadequate catalyst performance in HTSC can diminish conversion rates and elevate the workload on LTSC. Catalyst in HTSC is replaced periodically during every Factory Turn Around to maintain the performance of HTSC device. Therefore, this research aimed to analyze the performance of catalyst life based on the percent CO conversion, temperature, and pressure drop parameters. The objective is to determine the most effective duration for using HTSC catalyst.

2. Research Methods

The analysis of catalyst lifetime in HTSC (104-D1) process unit at PUSRI II-B Factory involved several stages of data collection. This included obtaining essential data such as design and actual data from June 2021 to November 2022. The evaluation flowchart of HTSC (104-D1) at the PUSRI II-B Factory is shown in Figure 2.

2.1 Primary Data

Primary data, obtained directly from the field during the operation of HTSC unit with a non-isothermal system, was collected from PUSRI-IIB ammonia factory data (Department of Operations and PUSRI-IIB Ammonia Control Room log sheet). Table 1 shows the design data obtained from PT. Pupuk Sriwidjaja Palembang handbook, including data on the operating conditions of the tool at factory start-up (initial factory start conditions).

Table 1. HTSC (104-D1) design data

Parameter	Inlet	Outlet
Temperature (°C)	371	431
CO (kmol/hr)	1660,981	507,854
CO_2 (kmol/hr)	1230,981	2384,175

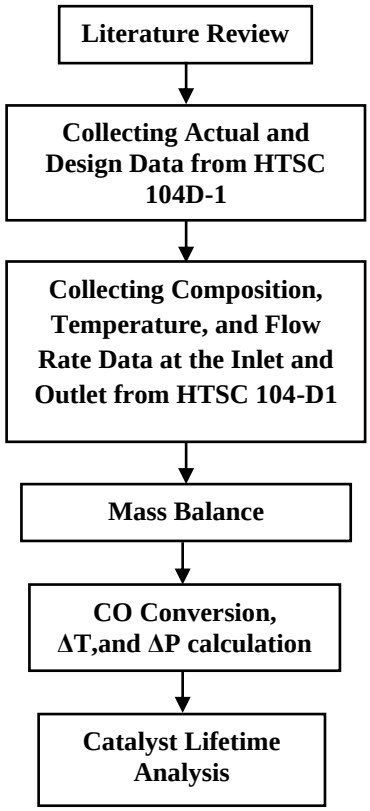

Figure 2. Flow diagram of catalyst lifetime analysis on HTSC (104-D1)

2.2 Secondary Data

Secondary data was obtained from several references such as handbook, journals, PUSRI website, and the philosophy of the production process. Calculation of CO to CO_2 conversion in HTSC (104-D1) follows Equation 1.

$$\% \, Conversion = \frac{Mol\ Outlet - Mol\ Inlet}{Mol\ Inlet} \times 100\% \quad \text{....(1)}$$

3. Results and Discussion

The reaction in HTSC is both reversible and exothermic, influenced by the elevated operating temperature observed at HTSC outlet. The performance of HTSC (104-D1) is affected by temperature, steam-to-gas ratio, pressure drop, and % CO in an outlet. An elevated steam-to-carbon (S/CO) ratio improves the conversion of CO_2 and H_2, resulting in a decrease in CO concentration. Under these conditions, the diminishing CO concentration shows a decline in equipment efficiency [10].

Catalyst used in a reaction, at a certain time, will have a decrease in activity, due to its age or lifetime. Catalyst life is defined as a period during which it produces the desired reaction product greater than the reaction product without a catalyst [12].

Water gas shift HTSC catalysts have been extensively examined and widely used industrially because of the low cost, long service life (3–5 years), and resistance to poisoning. They are usually operated in a temperature range of about 320–450 °C (non-isothermal system). Most HTSC catalysts are based on Fe_2O_3 (80–90 wt.%) and Cr_2O_3 (8–10 wt.%), with the balance being promoters/stabilizers (e.g. CuO_2, Al_2O_3, alkali, MgO, ZnO) [13].

Table 2. CO conversion, ΔT, and ΔP calculations of HTSC (104-D1)

No	Month	CO (kmol/h)		Conversion (%)	ΔT (^{O}C)	ΔP (kg/cm^2)
		Inlet	Outlet			
X	Design	1660.982	507.854	69.425	60.000	-
1	June 2021	1102.704	359.184	67.427	63.070	0.350
2	July 2021	1149.302	249.165	78.320	69.240	0.260
3	August 2021	1248.635	275.537	77.933	67.270	0.280
4	September 2021	1274.798	283.677	77.747	66.210	0.280
5	October 2021	1288.542	291.262	77.396	66.170	0.280
6	November 2021	1280.771	292.514	77.161	66.150	0.280
7	December 2021	1296.887	297.514	77.059	66.030	0.280
8	January 2022	1246.709	287.613	76.930	66.020	0.280
9	February 2022	1189.501	275.534	76.836	65.890	0.280
10	March 2022	1252.396	290.275	76.822	65.860	0.290
11	April 2022	1255.232	297.012	76.338	65.850	0.290
12	May 2022	1046.003	247.686	76.321	65.780	0.290
13	June 2022	1234.163	292.637	76.289	65.710	0.290
14	July 2022	1205.799	287.149	76.186	65.670	0.290
15	August 2022	1300.303	312.539	75.964	65.660	0.290
16	September 2022	1198.742	292.433	75.605	65.550	0.290
17	October 2022	1258.706	307.306	75.586	65.370	0.290
18	November 2022	1224.946	302.621	75.295	65.220	0.290

The Copper-Promoted Iron catalyst utilized in HTSC (104-D1) belongs to the Shift-Max 120 type, specifically designed for converting CO to CO_2 through the water shift reaction at operating conditions of 330–500ºC. Catalyst chemical composition includes Fe_2O_3 89%, Cr_2O_3 8%, CuO 1.8%, and sulfur less than 150 ppm [14]. The physical properties of the Copper-Promoted Iron catalyst are in the form of domed tablets with a density of 1.08 kg/L, a volume of 65 m^3, a mass of 70,200 kg, and a size of 6 x 6 mm.

Data for calculating catalyst lifetime analysis comprises both the design data of HTSC (104-D1) and the actual operational data, shown in Table 2. Table 2 shows the data obtained from June 2021 to November 2022. Catalyst performance in HTSC (104D-1) was still far above the design data. The Copper-Promoted Iron catalyst was replaced during Turn Around in June 2021, and serves as reference data for conditions pre-replacement.

Based on the observed data, the performance of catalyst in HTSC (104D-1) has decreased step by step. Subsequently, the June 2021 data, representing conditions before Turn Around, shows a performance below the design specifications, signaling the need for catalyst replacement. There are several parameters observed to investigate catalyst performance and lifetime. The parameters used are pressure drop (ΔP), temperature profile (ΔT), and percent CO conversion on HTSC (104D-1) [15].

3.1 Catalyst performance according to pressure drop (ΔP)

Pressure drop is an operating condition that can be used to review catalyst performance because the value of the pressure drop is related to the reaction conversion that occurs. A higher pressure drop tends to decrease reaction conversion, leading to unreacted reactants [16].

The pressure drop graph in Figure 3 shows a linear trend, implying that over time, the pressure drop increases. June 2021 pressure drop data serves as a reference due to the absence of available design data. This particular dataset is selected as a reference because it represents the last operating condition before Turn-Around. Subsequently, from July 2021 - November 2022, the value of the pressure drop tends to increase periodically, approaching the pressure drop value of the reference data. This condition shows that catalyst performance has decreased, specifically on the active side. According to the research conducted by Utomo & Laksono [17], it was reported that one of the causes of catalyst deactivation, namely fouling, occurred due to material clumping on the active side. The increase in the amount of relatively large deposits will close the active sites of catalyst, and fouling of catalyst will increase the pressure drop in the reactor.

A decrease in catalyst activity may stem from obstructed pores, creating a pressure difference between the inlet and outlet. Closed catalyst pores may result from compounds that act as poisons. These chemical compounds cover catalyst pores as their molecular size exceeds that of pores [18]. The closed catalyst pores will prevent CO gas from reacting with H_2O to form CO_2, causing a decrease in CO conversion from the design level. CO that escapes will exacerbate the performance of the next shift conversion process unit, namely LTSC (104D-2A/B).

Based on the graph obtained, the trendline is 0.655. This showed that the data obtained has sufficient validity to be

used as a review of catalyst performance evaluation. This means that 65.50% of the data is valid to show the performance of catalyst.

From the graph equation and using the goal-seek method, the remaining lifetime of catalyst can be predicted. By substituting the value 0.35 as y on the graph, the corresponding month shows when catalyst will reach a value of 0.35. From this data, the remaining lifetime is calculated as 3 years and 6 months. This implies that catalyst can continue to be used for the next 3.5 years, showing an actual catalyst lifetime of 4 years and 11 months since catalyst replacement.

According to the data, the lower process conditions affect lifetime of the use of catalyst. This is also supported by the condition of the pressure drop which is still below the reference. The use of catalysts for many years will result in the accumulation of these catalyst-toxic compounds increasing every year. Although the actual concentration is very small and negligible, it can lead to large accumulations over several years. The result is that catalyst will be deactivated [19].

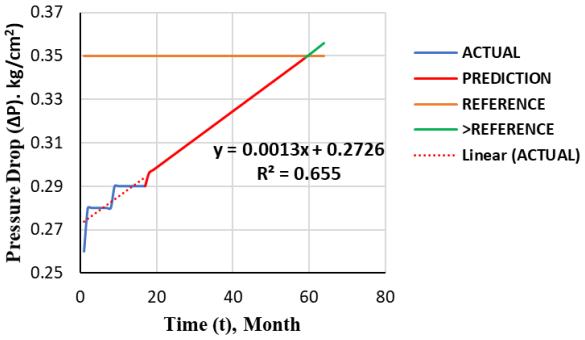

Figure 3. Effect of time on pressure drop

3.2 Catalyst performance according to temperature (ΔT)

Temperature is an integral factor in chemical reactions, particularly in industrial processes. It is closely tied to the minimum energy required to initiate a chemical reaction, known as activation energy [18]. The reaction in HTSC is exothermic. In an exothermic reaction, the enthalpy value of the reactants is greater than the enthalpy of the products, which results in the release of heat from the system to the surroundings. Therefore, the increase in temperature in HTSC shows that a reaction has occurred in the process equipment.

Achieving a high CO conversion percentage is possible with low operating temperatures, but it is crucial to maintain the temperature above the steam condensation point. An increase in the temperature profile causes the equilibrium to shift to the left, thereby CO exit is greater, but kinetically, the high temperature can accelerate the reaction rate and approach conversion at equilibrium conditions [20]. Elevated temperatures are problematic as they can harm the HTSC catalyst, leading to reduced performance. Maintaining an optimal temperature is crucial for the efficient conversion of CO to CO2, preventing issues such as catalyst deactivation through sintering. Sintering results in a decreased contact surface area, consequently diminishing catalyst activity [5].

Based on the graph in Figure 4, the actual data tends to form a linear line, the trendline of the graph obtained is 0.5498. This shows that the data obtained has sufficient validity to be used as a review of catalyst performance evaluation. This means that 54.98% of the data is valid to show the performance of catalyst. The

actual data for July 2021 – and November 2022 appears quite distant from the design data which shows that HTSC catalyst is still functioning properly starting from catalyst replacement period until November 2022.

According to the graph equation and using the goal-seek method, the remaining catalyst lifetime can be predicted. Substituting a y-value of 60 into the graph predicts a remaining catalyst lifetime of 3 years. Consequently, catalyst is projected to be usable for the next 3 years, contributing to a total catalyst lifetime of 4 years and 5 months. This estimation guides considerations for catalyst replacement. The difference in lifetime is due to the small percentage of data validation. Despite their differences, they can be taken into account when considering catalyst replacement.

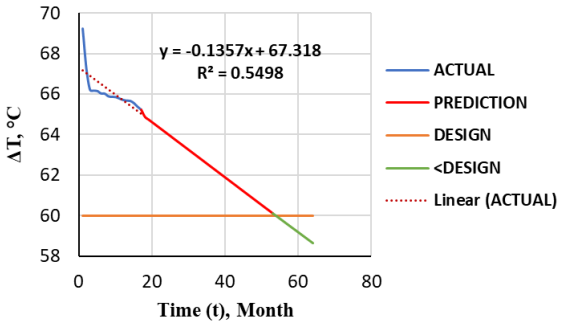

Figure 4. The effect of time on the temperature

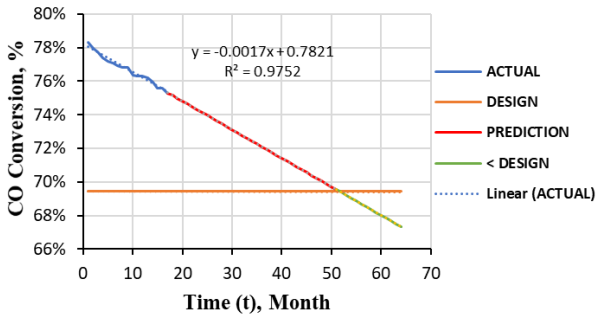

Figure 5. Effect of time on CO conversion

3.3 Catalyst performance according to CO conversion

Conversion shows the extent to which the reactants transform into products, serving as a crucial indicator for catalyst performance. Various operating conditions, including pressure drop, influence conversion. A higher pressure drop correlates with lower reaction conversion in the process [16]. Based on PT. Pupuk Sriwidjaja handbook, the shift converter targets around ±70% CO conversion in HTSC, with nearly perfect CO conversion in LTSC. The design data shows a conversion value of 69.42% which is quite appropriate. However, data for June 2021 shows a value of 67.43% which shows that the performance of catalyst is below the design data.

Based on the graph in Figure 5, the actual data tends to form a linear line, the trendline of the graph obtained is 0.9752. This shows that the data obtained has great validity to be used as a review of the catalyst performance evaluation. This means that 97.52% of the data is valid to show the performance of catalyst. Actual data for July 2021 - November 2022 appears quite distant from the design data, which shows that HTSC catalyst is still functioning properly starting from catalyst replacement period until November 2022.

From the graph equation and using the goal-seek method, the remaining lifetime of the catalyst can be predicted. Substituting a y-value of 69.42 into the graph predicts a remaining catalyst lifetime of 3 years. This projection shows that catalyst is expected to remain effective for the next 3 years, providing valuable information for ongoing usage and replacement considerations.

In June 2021, the Turn Around operation aimed to clean equipment and

replace catalysts on the HTSC bed, to enhance production efficiency and increase CO conversion. Data for June 2021 showed a conversion value of about 67.43%, despite being below the designed value, this data remained valuable as a reference since it represents the latest information just before catalyst replacement. Substitute 67.43 for y on the graph to determine when the catalyst value reaches 67.43. With this information, the catalyst has a remaining lifetime of 3 years and 10 months, showing that it can be used for a total of 4 years and 8 months.

The data shows that the catch unit can still operate with a conversion percentage below the design data, although it is still about ±70%. The consequence of this is an increased workload for LTSC, the subsequent shift converter unit. The observed decrease in conversion suggests a potential decline in catalyst activity. Concurrently, a reduction in conversion implies a decrease in catalyst activity [21]. The actual conversion, however, is not only influenced by catalyst activity but also by factors such as pressure drop, amount of incoming feed, flow rate, etc. [22]. There is a direct relationship between catalyst activity and conversion. If catalyst activity decreases, it leads to a subsequent decrease in the reaction conversion in the shift converter [23].

4. Conclusion

In conclusion, this research showed that pores on the active side of the catalyst produce a greater pressure drop (ΔP), which lowers the CO conversion percentage and degrades catalyst performance. The increase in temperature (ΔT) in HTSC showed an exothermic reaction that occurred. The optimal reaction rate occurred at a high temperature, while the equilibrium occurred at a low temperature. CO conversion is directly proportional to HTSC catalyst performance, with decreased conversion signaling a decline in catalyst effectiveness. Catalyst on HTSC (104-D1) can be used for 4 years and 8 months after its replacement.

References

[1] Aziz, M., TriWijayanta, A., & Nandiyanto, A. B. D. (2020). Ammonia as effective hydrogen storage: A review on production, storage and utilization. *Energies*, 13(12), 3062. doi: 10.3390/en13123062

[2] PT Pupuk Sriwidjaja Palembang (Pusri). (2023). Anhydrous ammonia. *Ammonia Product*. Retrieved from https://www.pusri.co.id/en/product/ammonia/anhydrous-ammonia

[3] Felder, R. M., Rousseau, R. W. (2009). *Elementary Principles of Chemical Processes*. (L. Linda, Ed.)*John Wiley & Sons, Inc* (4th ed.). United States of America: Laurie Rosatone.

[4] PT Pupuk Sriwidjaja Palembang (Pusri). (2017). *Filosofi proses pabrik ammonia PUSRI – IIB kapasitas produksi 2000 MTPD* (2nd ed.). Palembang: PT. Pusri Palembang.

[5] Pal, D. B., Chand, R., Upadhyay, S. N., & Mishra, P. K. (2018). Performance of water gas shift reaction catalysts: A review. *Renewable and Sustainable Energy Reviews*, 93, 549–565. doi: 10.1016/j.rser.2018.05.003

[6] Kohout, J. (2021). Modified arrhenius equation in materials science, chemistry and biology. *Molecules*, 26(23), 1–19. doi: 10.3390/molecules26237162

[7] Ojelade, O. A., & Zaman, S. F. (2021). Ammonia decomposition for hydrogen production: a thermodynamic study. *Chemical Papers*, 75(1), 57–65. doi: 10.1007/s11696-020-01278-z

[8] Chen, W. H., & Chen, C. Y. (2020). Water gas shift reaction for hydrogen production and carbon dioxide capture: A review. *Applied Energy*, 258, 1–25. doi: 10.1016/j.apenergy.2019.114078

[9] Benny, S. (2010). *High Temperature Water Gas Shift Catalysts : A Computer Modelling Study*.

Johnson Matthey Technology Centre. University College London.

[10] Patra, T. K., Mukherjee, S., & Sheth, P. N. (2019). Process simulation of hydrogen rich gas production from producer gas using HTS catalysis. *Energy*, 173, 1130–1140. doi: 10.1016/j.energy.2019.02.136

[11] Zhang, Z., Wu, Z., Rincon, D., & Christofides, P. D. (2019). Operational safety of an ammonia process network via model predictive control. *Chemical Engineering Research and Design*, 146, 277–289. doi: 10.1016/j.cherd.2019.04.004

[12] Hughes, R. (1989). Activation, Deactivation and Poisoning of Catalysts. *Chemical Engineering Science*, 44(8), 1747–1748. doi: 10.1016/0009-2509(89)80018-1

[13] Shekhawat, D., Spivey, J. J., & Berry, D. A. (2011). *Fuel Cells: Technologies for Fuel Processing*. *Fuel Cells: Technologies for Fuel Processing*. Amsterdam: Elsevier Science. doi: 10.1016/C2009-0-20328-X

[14] Baboo, P. (2015). Catalyst in Amonia Plant and Their PerformanceEvaluation. National fertilizers Ltd, India.

[15] Wahdaniyah, N. (2018). *Evaluasi Kinerja Katalis Methanator (106-D) Unit Amonia Operasi Pabrik-2 Pt. Pupuk Kalimantan Timur-Bontang*. Politeknik Ati Makassar.

[16] Schmidt, L. D. (2005). *Engineering of Chemical Reactions*. *Engineering of Chemical Reactions* (2nd ed.). New York: Oxford University Press.

[17] Utomo, M. P., & Laksono, E. W. (2007). Tinjauan umum tentang deaktivasi katalis pada reaksi katalisis heterogen. In *Prosiding Seminar Nasional Penelitian, Pendidikan, dan Penerapan MIPA* (pp. 110–115). Yogyakarta: Universitas Negeri Yogyakarta.

[18] Suarsa, I. W. (2017). Teori Tumbukan Pada Laju Reaksi Kimia. *Pengembangan Bahan Ajar*. Denpasar: Jurusan Teknik Kimia, FMIPA, Universitas Udayana.

[19] Dunleavy, J. K. (2006). Sulfur as a catalyst poison. *Platinum Metals Review*, 50(2), 110. doi: 10.1595/147106706X111456

[20] Uningtya, N. (2018). *Evaluasi kinerja katalis pada high temperature shift converter dan low temperature shift converter (104-D) di unit amonia PUSRI-IV*. Univesitas Pembangunan Nasional "Veteran" Yogyakarta.

[21] Baraj, E., Ciahotný, K., & Hlinčík, T. (2022). Advanced Catalysts for the Water Gas Shift Reaction. *Crystals*, 12(4), 509. doi: 10.3390/cryst12040509

[22] Dey, S., & Mehta, N. S. (2022). Low temperature catalytic conversion of carbon monoxide by the application of novel perovskite catalysts. *Science in One Health*, 1. doi: 10.1016/j.soh.2022.100002

[23] Farah, E., Demianenko, L., Engvall, K., & Kantarelis, E. (2023). Controlling the Activity and Selectivity of HZSM-5 Catalysts in the Conversion of Biomass-Derived Oxygenates Using Hierarchical Structures: The Effect of Crystalline Size and Intracrystalline Pore Dimensions on Olefins Selectivity and Catalyst Deactivatio. *Topics in Catalysis*, 66, 1310–1328. doi: 10.1007/s11244-023-01833-4

CHEESA: Chemical Engineering Research Articles
ISSN **2614-8757 (Print)**, ISSN **2615-2347 (Online)**
Available online at: http://e-journal.unipma.ac.id/index.php/cheesa

Research Article

The Effect of NaOH Concentration and Acetylation Time on Synthesis of Kepok Banana Peel Cellulose Acetate

Pengaruh Konsentrasi NaOH dan Waktu Asetilasi Terhadap Sintesis Selulosa Asetat Kulit Pisang Kepok

Fia Kharisma Yasmin[1)], Ayu Pramita[1*)], Dodi Satriawan[1)]

[1)]Politeknik Negeri Cilacap, Environmental Pollution Control Engineering, Indonesia

Article History
Received: 23th July2023; Revised: 10th December2023; Accepted: 12th December2023; Available online: 04th January 2024; Published Regularly: December 2023

doi: 10.25273/cheesa.v6i2.17294.85-94

*Corresponding Author.
Email: ayu164606@gmail.com

Abstract

The high production of kepok banana is generating a significant amount of peel waste, contributing to environmental pollution. To address this issue, an innovative solution is the conversion of kepok banana peel into cellulose acetate as raw material for membrane production. Therefore, this research aimed to manufacture kepok banana peel cellulose acetate using varying concentrations of 1%, 1.5%, and 2% NaOH solvent, with acetylation times of 2 hours and 2.5 hours, respectively. The optimal results were achieved using 1% NaOH with kepok banana peel cellulose content of 56.07%. Furthermore, the best acetylation time occurred at a duration of 2.5 hours, producing a cellulose acetate content of 38.23% and a 2.3% degree of substitution (DS). These results suggested that the optimal combination for producing membrane from kepok banana peel is 1% concentration with an acetylation time of 2.5 hours, classifying it as cellulose diacetate.

Keywords: acetylation; cellulose; cellulose acetate; delignification; Kepok banana peel

Abstrak

Tingginya produksi kulit pisang kepok menghasilkan limbah kulit pisang yang mencemari lingkungan. Salah satu solusi dan inovasi untuk mengatasi permasalahan tersebut adalah dengan mengolah kulit pisang kepok menjadi selulosa asetat sebagai bahan baku pembuatan membran. Pembuatan selulosa kulit pisang kepok menggunakan variasi konsentrasi pelarut NaOH 1%, 1,5% dan 2%. Sedangkan pembuatan selulosa asetat dari kulit pisang kepok menggunakan variasi waktu asetilasi 2 jam dan 2,5 jam. Hasil penelitian terbaik terdapat pada pelarut NaOH 1% dengan kadar selulosa kulit pisang kepok sebesar 56,07%. Waktu asetilasi terbaik yaitu 2,5 jam menghasilkan kadar selulosa asetat sebesar 38,23% dan derajat substitusi sebesar 2,3%. Berdasarkan hasil penelitian, selulosa asetat 1% dengan waktu asetilasi 2,5 jam merupakan jenis selulosa diasetat untuk pembuatan membran selulosa asetat kulit pisang kepok.

***Kata kunci**: asetilasi; delignifikasi; kulit pisang kepok; selulosa; selulosa asetat*

1. Introduction

Indonesia is widely recognized for its extensive natural resources and holds a significant position as a leading banana producer globally. Generally, banana is a fruit plant, consisting of roots, stems, leaves, fruit flesh, and peel. The volume of banana production in the country from 2013 to 2017 was 6,279,279 tons, 6,862,558 tons, 7,299,266 tons, 7,007,117 tons, and 7,162,678 tons, respectively [1]. Among popular varieties, kepok banana (*Musa balbisiana*) is widely used for its meat as a processed food. However, the community has not fully optimized the use of kepok banana peel, resulting in immediate disposal as waste in the environment. This phenomenon contributes to environmental pollution and disrupts the aesthetics of the surrounding community. In order to address this issue, kepok banana peel is converted into cellulose acetate as raw material for membrane production.

Cellulose acetate membrane has become a significant technology in the field of renewable microfiltration membranes, currently gaining attention and rapid development globally [2]. This membrane is made of a natural polymer that has been developed as an alternative to conventional separation processes [3]. The natural polymer materials used in the manufacturing process are cellulose and cellulose acetate. Moreover, cellulose is obtained from kepok banana peel waste, which is used to manufacture membrane, consisting of 60-65% cellulose, 6-8% hemicellulose, and 5-10% lignin. Cellulose can be made into cellulose acetate through acetylation reactions [4]. Kepok banana peel waste is also processed into cellulose acetate by varying the speed of stirring through the acetylation process [5].

Cellulose acetate has distinct characteristics, including an asymmetric structure with an ultra-thin active layer, capable of retaining dissolved materials on a rough support layer. Furthermore, it is resistant to precipitation, producing biodegradable, hydrophilic, and hydrophobic properties for use as a raw material in membrane production. Cellulose acetate has a chemical property that allows it to dissolve in acetone [6][7]. The use of agar processing waste offers a viable pathway to produce cellulose acetate. This process uses various solvents such as NaOH at 3%, 6%, and 9% during isolation and variations in the ratio of cellulose acetate anhydride in the acetylation. The results showed that 6% NaOH could produce a hemicellulose content of 24.92% and the highest 53.33% alpha cellulose with a 24.92% yield value. The optimal ratio of cellulose and acetic anhydride to obtain cellulose acetate is 1:10, showing a whiter cellulose acetate color with a yield of 26.19% and an acetyl content of 43.5% [8]. The conversion of coconut coir into cellulose acetate has also been carried out, with varying volumes of acetic anhydride. The results showed that a maximum volume of 60 ml yielded an acetic anhydride with an acetyl content of 50.8737% and a Degree of Substitution (DS) of 3.8126% [9]. Another study has used empty palm fruit bunch pulp as a cellulose acetate product. The results obtained cellulose acetate levels ranging from 18-48% with an optimum acetylation time of approximately 2–3.5 hours [10]. Waste from cassava stems has been found effective in cellulose acetate production, yielding a content of 41.01%, and classified as cellulose diacetate [11].

Based on the problems above, this research aimed to apply kepok banana peel

waste in the manufacturing of cellulose acetate as a raw material for membrane production. The novelty is variations in the concentration of NaOH solvent (1%, 1.5%, and 2%) in the delignification process and acetylation time. A NaOH solvent with a higher concentration causes the degradation of cellulose, leading to a decrease in cellulose levels in the delignification process. The percentage of cellulose acetate content increased to a maximum at an acetylation time of 2.5 hours. However, prolonged acetylation reaction time results in decreased cellulose acetate content, showing a direct proportionality to the DS [12][13]. This research is anticipated to minimize kepok banana peel waste and obtain optimal cellulose acetate as a raw material for cellulose acetate membrane production.

2. Research Methods

2.1 Instruments and Materials

The kepok banana peel was obtained from a fried banana seller in Cilacap. The chemicals used include NaOH, CH_3COOH, $(CH_3CO)_2O$, and H_2SO_4 obtained from Merck, while NaOCl and Aquadest were collected from Brataco. The instrument was glassware, sieve 60 mesh, analytical balance, Fourier Transform Infra-Red (FTIR) specification Bruker Alpha II Platinum-ATR, and Scanning Electron Microscope (SEM) merk Tescan.

2.2 Preparation of Cellulose

The preparation of kepok banana peel cellulose commenced with a delignification process to remove the lignin and hemicellulose content, obtaining a high cellulose content. Kepok banana peel measuring 60 mesh and 50 grams was added to a 1% NaOH solution and refluxed at 70^{o}C for 2 hours. The precipitate of kepok banana peel was filtered and washed using distilled water to achieve a neutral pH of 6.5–7.5. This was followed by bleaching the delignified peel with a 1.75% NaOCl solution, using a sample-to-NaOCl solution ratio of 1:25, and heating at 70^{o}C for 1 hour. Subsequently, filtration and neutralization were carried out using distilled to obtain a neutral pH. The cellulose content and functional groups were analyzed using the FTIR instrumentation and the surface structure with the SEM on delignified kepok banana peel.

2.3 Preparation of Cellulose Acetate

The preparation of cellulose acetate was carried out by mixing 75 grams of wet cellulose powder with 150 ml of a 30% glacial acetic acid solution, followed by heating, and stirring at 38^{o}C for 60 minutes. Approximately 1 ml of a 2% sulfuric acid solution was added, heated, and stirred at the same conditions. Furthermore, the acetylation process was carried out by adding 40 ml of a 30% acetic anhydride solution, heating, and stirring at 38^{o}C, with variations lasting for 2 and 2.5 hours, respectively. This was followed by the addition of 10 ml of distilled water and 20 ml of a 30% glacial acetic acid solution, which was heated and stirred at 50^{o}C for 30 minutes. The solution was allowed to stand, forming a precipitate, which was placed in 500 ml of distilled water to achieve white cellulose acetate flakes. The cellulose acetate was filtered and neutralized using distilled water until the sour smell disappeared. Subsequently, cellulose acetate content and Degree of Substitution (DS), functional groups were also analyzed using the FTIR, and the surface structure of the cellulose

acetate was measured with SEM instrumentation.

3. Results and Discussion

3.1 Kepok Banana Peel Cellulose

In this research, kepok banana peel cellulose was produced through delignification, bleaching, and washing processes. The delignification process using NaOH solvent was carried out to reduce the lignin and hemicellulose content. Delignification produced cellulose, which was distinguished by a blackish brown color, as moist powder kepok banana peel. The bleaching process was performed to whiten the cellulose content, which has a blackish-brown color from the results of delignification. After the cellulose was washed with distilled water to neutralize its pH, which ranged from 6.5 to 7, a white, odorless product was produced. Figure 1 shows the results of delignification and bleaching in the form of cellulose from kepok banana peel waste.

(a) **(b)**

Figure 1. Delignification of kepok banana peel cellulose a) before bleaching; b) after bleaching

The analysis of the cellulose content of kepok banana peel was carried out using the Chesson method [13]. Based on the results, the cellulose content was found to be 56.07%, 46.54%, and 44.54%, in 1%, 1.5%, and 2% NaOH solvent. This showed that the interaction between lignin compounds and NaOH solvents produced the best results at a concentration of 1%. The lignin content in the kepok banana peel was degraded due to an increase in the cellulose content of the kepok banana peel. This suggested that NaOH with a higher concentration would cause the degradation of cellulose, thereby leading to a decrease in the cellulose content obtained in the extraction results [12][13].

Functional group analysis was carried out to identify the presence of functional groups and wave numbers based on the bonds contained in the cellulose of the kepok banana peel. Subsequently, tests were carried out using the Bruker Alpha II Platinum-ATR FTIR instrumentation at the Engineering Laboratory of Politeknik Negeri Cilacap. Figure 2 shows the results of the analysis of functional groups and wave numbers formed in kepok banana peel cellulose from delignification with 1%, 1.5%, and 2% NaOH solvent variations.

Based on Figure 2, it was discovered that 1% NaOH solvent showed the absorption of functional groups typical for cellulose compounds. The absorption depth at wave number 3334.03 cm^{-1} indicated the presence of the O-H stretch functional group, and wave number 2850.11 cm^{-1} proved the presence of the C-H stretch functional group. Furthermore, the absorption depth of wave numbers 1462.26 cm^{-1} and 1159.88 cm^{-1}, showed the existence of the CH_2 bend and C-H bend functional group. The absorption depth of 1036.84 cm^{-1} wave numbers proved the existence of the C-O stretch functional group.

The functional group and wave number analysis of cellulose kepok banana peel with 1.5% NaOH variations also demonstrated the absorption of functional

groups that are characteristic of cellulose compounds. The absorption depth at wave number 3328.88 cm^{-1} indicated the presence of the O-H stretch functional group and C-H at 2851.32 cm^{-1}. Furthermore, the absorption depth of wave numbers 1374.60 cm^{-1} and 1156.15 cm^{-1}, indicated the presence of the CH_2 bend and C-H bend functional groups. The absorption depth of 1032.23 cm^{-1} wave numbers showed the existence of the C-O stretch functional group.

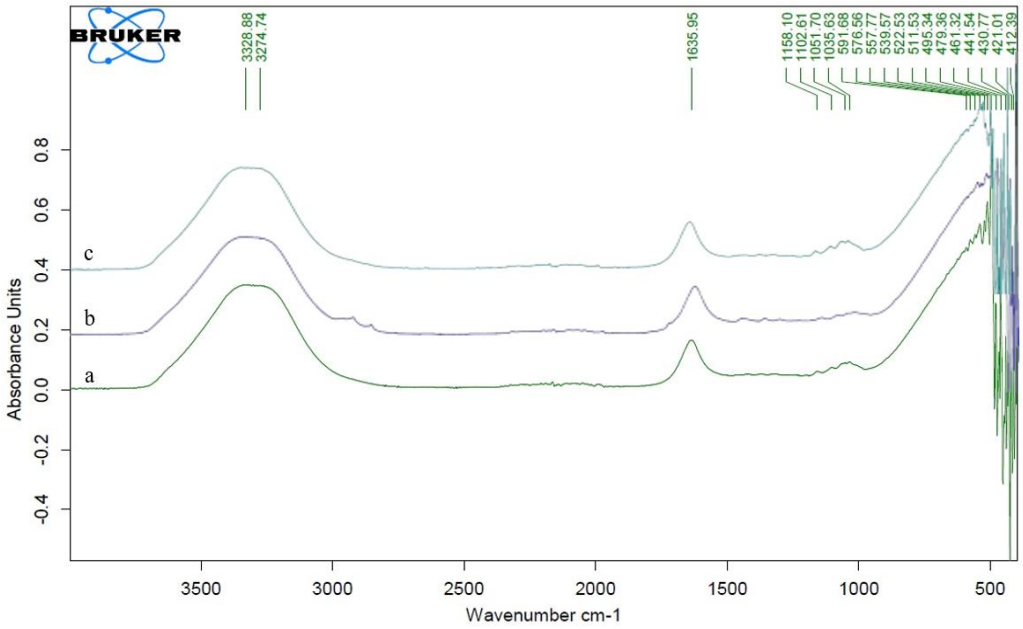

Figure 2. FTIR spectra of kepok banana peel cellulose with various concentration NaOH solvents a) 1%; b) 1.5% and c) 2%

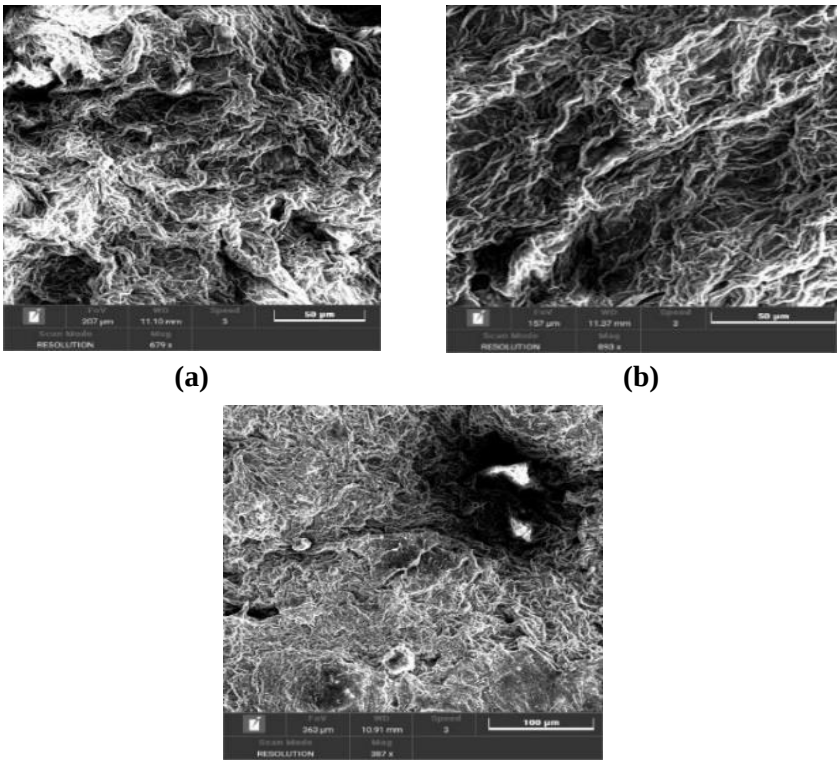

(a) **(b)**

(c)

Figure 3. Surface structure of kepok banana peel cellulose with NaOH solvent variations a) 1%; b) 1.5% and c) 2%

The analysis results of functional groups and wave numbers of cellulose kepok banana peel with variations in the 2% NaOH solvent showed the absorption of cellulose compounds. The absorption depth at wave number 3335.24 cm^{-1} indicated the presence of the O-H stretch functional group, while 2163.74 cm^{-1} showed C-H stretch. Furthermore, the absorption depth of wave numbers 1634.77 cm^{-1} and 1158.99 cm^{-1}, proved the existence of the CH_2 bend and C-H bend functional groups. The absorption depth of 1035.29 cm^{-1} wave numbers indicated the existence of the C-O stretch functional group.

Figure 3 shows the analysis of the surface structure of cellulose kepok banana peel resulting from delignification of 1%, 1.5%, and 2% NaOH solvent variations. The analyses were carried out using the SEM instrumentation of the Tescan brand located at the Environmental Physics Laboratory of Politeknik Negeri Cilacap.

Figure 3 (a) shows that the surface structure of 1% cellulose is smoother, with more fibers and a hollow structure, as observed at Mag 679x magnification. Furthermore, 1.5% concentration as presented in Figure 3 (b) shows a widened and fibrous pore surface structure observed with Mag 893x magnification. A 2% concentration, as illustrated in Figure 3 (c) showed a flat and dense fiber surface structure at magnification 387x. Based on the results, it was concluded that cellulose with 1% NaOH solvent produced the optimal surface structure.

3.2 Kepok Banana Peel Cellulose Acetate

In this study, an acetylation method with 2 and 2.5 hours variations was used to create the cellulose acetate of kepok banana peel. acetylation is a chemical reaction in which a different substance is substituted for the acetyl group.

During the acetylation process, a solution of acetic acid anhydride is used as a reagent, where the cellulose reacts with acetic anhydride to form cellulose acetate. Sulfuric acid is used as a catalyst to add a positive charge to the acid, accelerating the reaction and lowering the activation energy. Consequently, chemical reactions occur more easily and acetyl groups can be substituted by hydroxyl groups [9]. In cellulose acetate, the hydroxyl group is replaced by an acetyl group in the form of a white, tasteless, non-toxic, and odorless solid. In this research, the synthesis of cellulose acetate from kepok banana peel obtained a white and odorless product, as shown in Figure 4.

Figure 4. Kepok Banana Peel Cellulose Acetate

The analysis of cellulose acetate content and DS of kepok banana peel was carried out at 1% NaOH solvent and varying acetylation times of 2 hours and 2.5 hours. Moreover, the analysis was performed to determine the type of cellulose acetate produced in this research, including monoacetate, diacetate, or triacetate. At 1% NaOH solvent and an acetylation time of 2 hours, the results showed that the cellulose acetate content was 34% with a DS of 1.9%. Meanwhile, 1% NaOH solvent at 2.5 hours obtained a

content of 38.23% and 2.3% DS. An increasing trend was also observed in acetylation time as the cellulose acetate and the DS of kepok banana peel increased. The maximum increase in cellulose acetate levels occurred at 2.5 hours of acetylation time. Moreover, longer acetylation reaction time resulted in reduced cellulose acetate content [10][14]. The content of cellulose acetate is directly proportional to DS, with a higher value causing an increase in its melting point. Previous studies have established that the melting point of cellulose acetate ranged from 170 to 240°C. In this research, it was discovered that concentration at 1% NaOH solvent and acetylation time of 2.5 hours served as a type of cellulose diacetate effective for the production of membrane from kepok banana peel [15].

The functional group analysis was carried out to identify the presence of functional groups and wave numbers based on the bonds contained in the cellulose acetate of kepok banana peel, as shown in Figure 5.

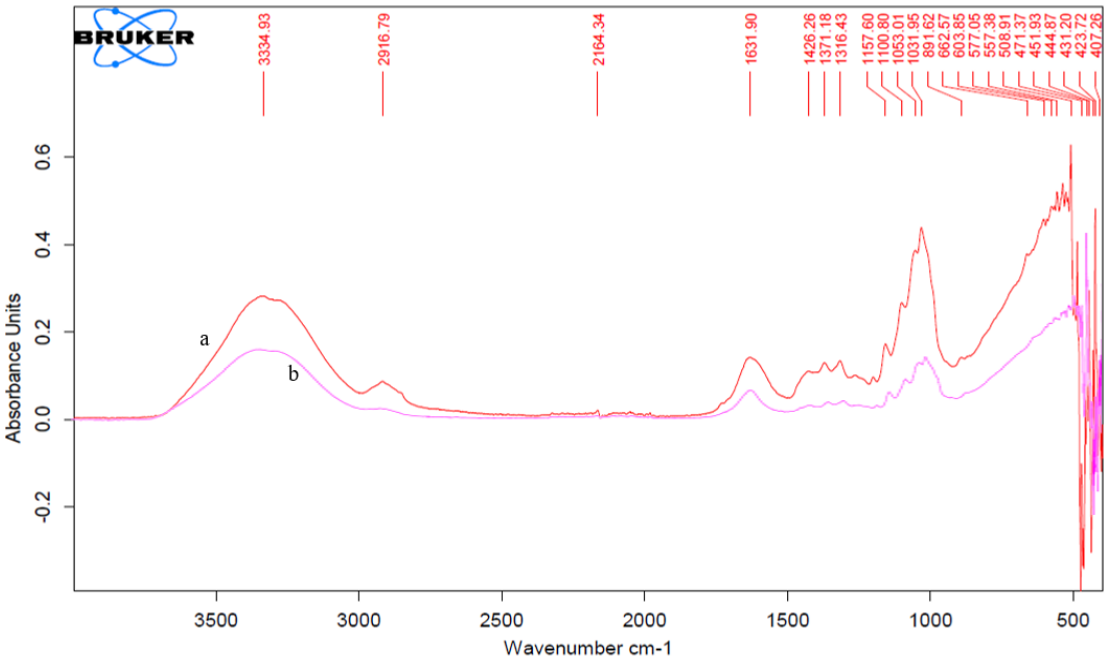

Figure 5. FTIR spectra of kepok banana peel cellulose acetate in 1% NaOH solvent with variations in acetylation time a) 2 hours and b) 2.5 hours

Table 1. Functional group of kepok banana peel cellulose acetate with 1% NaOH and acetylation time

Functional Groups	Wave Number (cm^{-1})*	Commercial Cellulose Acetate (cm^{-1})*	Acetylation Time	
			2 Hours (cm^{-1})	2.5 Hours (cm^{-1})
O – H Strectch	3750 – 3000	3486.97	3334.93	3328.12
C – H Strectch	3000 – 2700	2960.38	2916.79	2916.22
CH_2 Bend	1475 – 1300	-	1426.26	1429.75
C – H Bend	1300 – 1000	1383.89	1157.60	1263.64
C – O Strectch	1050 – 1000	-	1031.95	1033.03

**Source:* [8]

Figure 5 shows the analysis of functional groups and wave numbers of cellulose acetate from kepok banana peel in 1% NaOH solvent with acetylation time of 2 hours. Based on the results, a typical absorption of functional groups in the cellulose acetate compound was observed. The absorption depth at wave number 3334.93 cm^{-1} showed the presence of the O-H stretch functional group, while 2916.79 cm^{-1} indicated C-H stretch. Furthermore, the absorption depth of wave numbers 1426.26 cm^{-1} and 1157.60 cm^{-1} showed CH_2 and C-H bend functional groups, respectively. The absorption depth of 1031.95 cm^{-1} wave numbers indicated the existence of the C-O stretch functional group. The results of the FTIR spectrum analysis of cellulose acetate from kepok banana peel in 1% NaOH solvent with variations in the acetylation time of 2.5 hours above also showed the presence of functional group absorption in the cellulose acetate compound. At wave number 3328.12 cm^{-1}, the presence of O-H stretch was indicated, while 2916.22 cm^{-1} showed C-H stretch functional group. The absorption depth of wave numbers 1429.75 cm^{-1} and 1263.64 cm^{-1} indicated the existence of the CH_2 bend and C-H bend functional groups. Meanwhile, the absorption depth of 1033.03 cm^{-1} wave numbers indicated the presence of the C-O stretch functional group [16]. Table 1 further illustrates the functional groups of kepok banana peel cellulose acetate in 1% NaOH solvent at acetylation times of 2 hours and 2.5 hours.

The analysis of the surface structure of kepok banana peel cellulose acetate at varying acetylation times of 2 hours and 2.5 hours is shown in Figure 6. Cellulose acetate with 1% NaOH solvent and acetylation time of 2 hours showed a flat top surface, characterized by several spots resembling raisins when viewed with Mag 108 x magnification. Furthermore, cellulose acetate with 1% NaOH solvent and acetylation time of 2.5 hours showed a regular structure and hollow fibers with a magnification of 3.52 kx. In this research, the optimal results of surface structure analysis were obtained at a concentration of 1% NaOH solvent and an acetylation time of 2.5 hours.

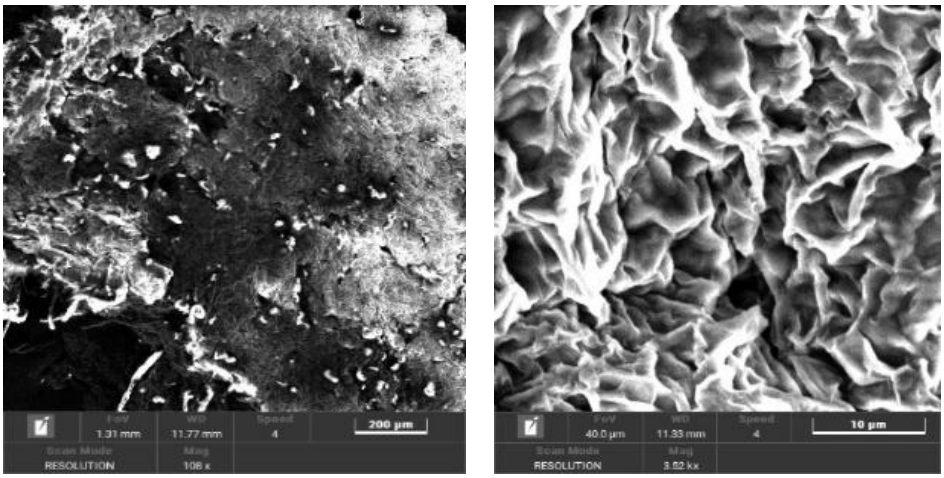

(a) **(b)**

Figure 6. Surface structure of cellulose acetate kepok banana peel variation acetylation time a) 2 hours and b) 2.5 hours

4. Conclusion

In conclusion, this research showed that the optimal cellulose content of kepok banana peel was obtained at 56.07% in 1% NaOH solvent, with a smoother surface structure, more fiber, and hollowness as observed with Mag 679 x magnification. At 2.5 hours of acetylation, the optimal yield was 38.23% cellulose acetate levels and a 2.3% degree of substitution. Based on these results, cellulose acetate with 1% NaOH solvent and acetylation time of 2.5 hours, served as a cellulose diacetate, which is suitable for membrane production from kepok banana peel.

5. Acknowledgments

The author is grateful for the assistance received from various parties, including Mrs. Theresia Evila Purwanti Sri Rahayu, S.T., M.Eng. as the Coordinator of the Applied Undergraduate Study Program in Environmental Pollution Control Engineering Politeknik Negeri Cilacap. Furthermore, the author is grateful to Mrs. Ayu Pramita, S.T., M.M., M.Eng. and Mr. Dodi Satriawan, S.T., M.Eng. who served as the supervising lecturers. This research was facilitated by the facilities and infrastructure of the Politeknik Negeri Cilacap Study Program of Environmental Pollution Control Engineering.

References

[1] BPS. (2022). Produksi Pisang Di Indonesia dari Tahun 2013-2017.

[2] Mirwan, A., Indriyani, V., & Novianty, Y. (2018). Pembuatan Membran Ultrafiltrasi Dari Polimer Selulosa Asetat Dengan Metode Inversi Fasa. *Konversi*, 6(1), 11. doi: 10.31213/k.v6i1.14

[3] Alvianto, D., Nurhadi, F. A. A., Putranto, A. W., Argo, B. D., Hermanto, M. B., & Wibisono, Y. (2022). Sintesis dan Karakterisasi Membran Selulosa Asetat dengan Penambahan Antibiofouling Alami Ekstrak Bawang Putih. *ALCHEMY Jurnal Penelitian Kimia*, 18(2), 193. doi: 10.20961/alchemy.18.2.57199.193-204

[4] Novianti, P., & Setyowati, W. A. E. (2016). Pemanfaatan Limbah Kulit Pisang Kepok Sebagai Bahan Baku Pembuatan Kertas Alami Dengan Metode Pemisahan Alkalisasi. *Prosiding Seminar Nasional Pendidikan Sains*, 459–466.

[5] Zhaafirah, H., & Fitriyano, G. (2017). Pengaruh Kecepatan Pengadukan Terhadap Rendemen dan Identifikasi Selulosa Asetat Hasil Asetilasi dari Limbah Kulit Pisang Kepok. *Jurnal Universitas Muhammadiyah Jakarta*, 008(November), 1–8.

[6] Seto, A. S., & Sari, A. M. (2013). Pembuatan Selulosa Asetat Berbahan Dasar Nata De Soya. *Konversi*, 2, 1–12.

[7] Syamsu, K., & Kuryani, T. (2014). Cellulose acetate biofilm production from microbial cellulose nata de cassava. *E-Jurnal Agroindustri Indonesia*, 3(1), 126–133.

[8] Nurhayati, N., & Kusumawati, R. (2014). Sintesis Selulosa Asetat dari Limbah Pengolahan Agar. *Jurnal Pascapanen dan Bioteknologi Kelautan dan Perikanan*, 9(2), 97. doi: 10.15578/jpbkp.v9i2.103

[9] Asparingga, H., Syahbanu, I., & Alimuddin, A. H. (2018). Pengaruh Volume Anhidrida Asetat Pada Sintesis Selulosa Asetat dari Sabut Kelapa (Cocos nucifera L.). *Jurnal Kimia Khatulistiwa*, 7(3), 10–17.

[10] Gaol, M., Sitorus, R., Yanthi, S., Surya, I., & Manurung, R. (2013). Pembuatan Selulosa Asetat Dari A -Selulosa Tandan Kosong Kelapa Sawit. *Jurnal Teknik Kimia USU*, 2(3),

33–39. doi: 10.32734/jtk.v2i3.1447

[11] Lismeri, L., Zari, P. M., Novarani, T., & Darni, Y. (2016). Sintesis Selulosa Asetat dari Limbah Batang Ubi Kayu. *Jurnal Rekayasa Kimia dan Lingkungan*, 11(2), 82–91.

[12] Silitonga, N., Tarigan, N., & Saragih, G. (2019). Pengaruh Konsentrasi NaOH pada Karakteristik α-Selulosa dari Pelepah Kelapa Sawit. *Jurnal Ready Star*, 2(1), 103–108.

[13] Kanani, N., Wardono, E. Y., Hafidz, A. M., & Octavani, H. R. (2018). Pengaruh Konsentrasi Pelarut Terhadap Proses Delignifikasi Dengan Metode Pre-Treatment Kimia. *Teknika: Jurnal Sains dan Teknologi*, 14(1), 87. doi: 10.36055/tjst.v14i1.5863

[14] Darmawan, M. T., Elma, M., & Ihsan, M. (2018). Sintesis Dan Karakterisasi Selulosa Asetat Dari Alfa Selulosa Tandan Kosong Kelapa Sawit. *Jukung (Jurnal Teknik Lingkungan)*, 4(1), 50–55. doi: 10.20527/jukung.v4i1.4658

[15] Souhoka, F. A., & Latupeirissa, J. (2018). Sintesis dan Karakterisasi Selulosa Asetat (CA). *Indo. J. Chem. Res.*, 5(2), 58–62. doi: 10.30598//ijcr.2018.5-fen

[16] Hariani, P. L., Riyanti, F., & Kurniaty, A. (2019). Modification of cellulose with acetic acid to removal of methylene blue dye. *Journal of Physics*, 1282, 1–8. doi: 10.1088/1742-6596/1282/1/012079

CHEESA: Chemical Engineering Research Articles
ISSN **2614-8757 (Print)**, ISSN **2615-2347 (Online)**
Available online at: http://e-journal.unipma.ac.id/index.php/cheesa

Research Article

Effect of EDTA Addition on Acidizing Treatment Process

Pengaruh Penambahan EDTA pada Proses Acidizing Treatment

Reno Fitriyanti[1,2*)], M.M. Lanny W. Pandjaitan[3)], Lukas[4)], Gilang Bagaskara Harlis[2)], Agus Wahyudi[2)], Muhrinsyah Fatimura[1,2)]

[1)]Universitas Katolik Indonesia Atma Jaya, Professional Engineer Program, Indonesia
[2)]Universitas PGRI Palembang, Chemical Engineering Department, Indonesia
[3)]Universitas Katolik Indonesia Atma Jaya, Electrical Engineering, Indonesia
[4)]Universitas Katolik Indonesia Atma Jaya, Cognitive Engineering Research Group (CERG), Indonesia

Article History
Received: 08th February 2023; Revised: 1st December2023; Accepted: 04th December2023; Available online: 11th January 2024; Published Regularly: December 2023

doi: 10.25273/cheesa.v6i2.15647.95-104

*Corresponding Author.
Email:
renofitriyanti@univpgri-palembang.ac.id

Abstract

Acidizing treatment is commonly used to solve scale problem on production equipment. In this process, Hydrochloric acid (HCl) is often used to treat $CaCO_3$ scale, posing the risk of pipe corrosion due to its high corrosive characteristics. Thus, the purpose of this study was to determine the impact of adding EDTA additive into HCl solution during the acidifying treatment procedure. The methodology included various stages such as scale identification, chemical scale removal test using 7.5% and 15% HCL solution, 15% HCl solution test with EDTA as an additive, and corrosion determination using corrosion coupon. The results showed that 15% HCl solution was very effective in removing $CaCO_3$ scale but had a high corrosion rate of 186.255 mpy. Furthermore, the addition of 10 mL EDTA solution as an additive removed scale and reduced corrosion rate by approximately 85%.

Keywords: acidizing treatment; EDTA; hydrochloric acid; scale

Abstrak

Acidizing treatment adalah metode yang umum digunakan dalam mengatasi masalah scale pada peralatan produksi. HCl merupakan jenis asam yang sering digunakan dalam mengatasi scale $CaCO_3$. Namun penggunaan HCl dapat menyebabkan korosi pada pipa karena memiliki sifat korosif yang tinggi. Penelitian ini bertujuan untuk menggetahui pengaruh penambahan zat additive EDTA dalam larutan HCl pada proses acidizing treatment. Tahapan penelitian dilakukan meliputi identifikasi scale, uji chemical scale dispersant menggunakan larutan HCl 7,5% dan 15%, uji larutan HCl 15% yang ditambah EDTA sebagai zat additive serta identifikasi korosi dengan corrosion coupon. Hasil penelitian menunjukkan larutan HCl 15% sangat efektif dalam menghilangkan scale $CaCO_3$, tetapi memiliki nilai laju korosi yang tinggi sebesar 186,255 mpy. Penambahan zat additive larutan EDTA sebesar 10 mL pada metode acidizing treatment mampu menghilangkan scale $CaCO_3$ dan mengurangi laju korosi hingga 85%.

Kata kunci: *acidizing treatment; asam klorida; EDTA; scale*

1. Introduction

Crude oil is a hydrocarbon compound that produces water, oil, and gas in the production process. As these three fluids flow to the surface, friction, changes in flow rate, and pressure cause scale formation on pipe walls [1]. Scale, corrosion, and emulsion are common production problems in oil field environments [2].

The presence of a crystal-shaped scale is closely related to the content of cations and anions in water formation [3]. It can form layers capable of reducing pipe diameter, decreasing the flow rate, and causing pipe blockages. Scale also results in corrosion due to the reaction of metal with ions adhering to the surface [4], causing an increase in pressure inside the pipe, leading to rupture [5].

Prevention and reduction of scale formation can be achieved by injecting chemical substances. To address the issue of scale formation, acidizing treatment, or acid stimulation, is a commonly used method [1]. This method includes injecting specific acids into production well to dissolve deposits or inhibit crust formation [6].

Hydrochloric acid (HCl) is commonly used to address scale issues in production pipe, serving as the most common solvent to dissolve $CaCO_3$ scale [7]. The reaction between HCl and carbonate effectively dissolves scale [8], posing the risk of pipe corrosion due to the high corrosiveness [9]. To address pipe corrosion when using HCl in acidizing treatment, an additive is introduced to act as an inhibitor [6].

Mixtures of organic acids can be used as additives to reduce the excessive corrosiveness of HCl [10]. The addition of consists of scale and corrosion coupons, organic substances is commonly applied to enhance the corrosion resistance of reinforced concrete in marine environments [11]. Organic compounds can also inhibit corrosion, specifically in acidic environments [12]. Previous research reported that the addition of organic substances such as oleic acid and arginine in acidizing treatment showed promising abilities in reducing corrosion rates [13][14]. However, the use of inorganic substances as corrosion inhibitors is limited due to environmental risks [15]. Organic compounds are a more environmentally friendly and efficient alternative to corrosion inhibitors in formation of adsorption films [16] [17].

The solution of Ethylene Diamine Tetraacetic Acid (EDTA) is a synthetic organic acid capable of forming bonds with various metal ions. The solution can adhere to the metal surface, acting as a coating that does not come into contact with the flow, thereby inhibiting metal oxidation and preventing corrosion [18].

Previous research showed that HCl solutions were available and efficient in addressing scale but may lead to corrosion on equipment. This limitation shows the need to investigate the effect of adding additives to acidizing treatments. Therefore, this research aimed to determine the impact of adding EDTA as an additive in acidizing treatment on scale solubility and corrosion rate in oil field production facilities.

2. Research Methods

2.1 Instruments and Materials

The instruments used in this research are corrosion and scale systems, as shown in Figure 1. Furthermore, the instrument including service valves and retrievers,

which function as the upper assembly to install and place coupons into the production pipe (flowline). Coupon holder was used to secure the voucher inside production pipe, followed by the cover for coupons and holder assembly. Other tools used include a pH meter and a DR 5000 spectrophotometer. The materials used included formation water samples, $CaCO_3$ scale obtained from the oil well production pipe (flowline), deionized water (aquades), NaOH, pH 10 buffer solution, EBT indicator, "Vario Ferro F10" reagent, potassium chromate indicator, $AgNO_3$, reagen “Vario Sulpha 4/F10”, reagent, scale dispersant (HCl), and the additive substance EDTA (Merck).

2.2 Research Stages

2.2.1 Scale Identification

Scale identification was conducted through the analysis of the ion content in formation water and measuring scales formed on production equipment. The ion content formed in formation water was analyzed using quantitative analysis, which included titrimetric and spectrophotometric analyses. The measurement was conducted by installing a scale coupon on production equipment. In the first step, the cover holder of coupon was opened and assembled with the service valve as well as the retriever. The service valve was installed at the designated point for placing coupon as presented in Figure 1. Subsequently, a coupon was placed on production pipe (flowline) for a specific period to obtain samples and scale size of the coupon.

2.2.1.1 pH Measurement

pH measurement was carried out by immersing the pH meter in formation water. Subsequently, the pH value was read when the instrument showed a stable number.

2.2.1.2 Calcium and Magnesium Content Measurement

The measurement of calcium ions (Ca^{2+}) and magnesium ions (Mg^{2+}) was performed using titration methods. A total of 10 mL of formation water sample was placed into a 100 mL volumetric flask and diluted with deionized water to 100 mL. Subsequently, 10 mL of diluted solution was mixed with 10 drops of 1 N NaOH solution and murexide indicator. The solution was titrated with a standard EDTA 0.02 N solution to achieve a color change from pink to purple (titrant volume = A). Subsequently, 1-2 mL of pH 10 buffer solution and 30-50 mg of EBT indicator/solution were added to 10 mL diluted sample solution. The solution was titrated with a standard EDTA 0.02 N solution until a red-to-violet color change occurred, turning blue (titrant volume = B). Ca^{2+} and Mg^{2+} content were calculated using Equations 1 and 2.

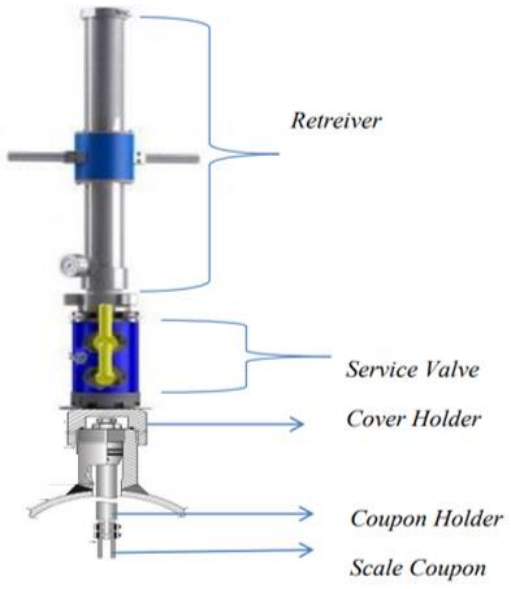

Figure 1. Corrosion and scale system

2.2.1.3 Measurement of Total Iron (Fe)

The measurement of iron ions were performed using a DR 5000 spectrophotometer. Initially, 10 mL of formation water was placed into a sample bottle with a diameter of 24 mm or 10 mm cuvette and tightly sealed. The sample bottle was placed in spectrophotometer sample slot and the instrument was calibrated by pressing the "ZERO" button. Subsequently, the sample bottle was removed, the "Vario Ferro F10" reagent was added, and it was tightly sealed and inverted to ensure a thorough mixture. This was followed by placing the sample slot and pressing the "TEST" button. After the reaction occurred for 3 minutes, the measurement results were displayed in mg/L.

2.2.1.4 Chloride Content Measurement

Chloride ion (Cl-) measurement was carried out using titration methods. Initially, 1 mL of 5% w/v potassium chromate indicator was added to the sample. This was followed by titration using the $AgNO_3$ solution until a color change from yellow to brick red occurred. Cl- concentration was calculated using Equation 3.

2.2.1.5 Barium Content Measurement

The measurement of barium ions was carried out using a DR 5000 spectrophotometer. A 100 mL sample of formation water was added to 5 mL of hydrochloric acid and heated until almost dry. Subsequently, the solution was diluted, and the absorbance was measured with a spectrophotometer. Barium content was calculated using Equation 4.

2.2.1.6 Sulphate Content Measurement

Sulphate ion (SO_4^{2-}) was measured using DR 5000 spectrophotometer. A 10 mL of formation water was placed into a sample bottle with a diameter of 24 mm or 10 mm cuvette and tightly sealed. The sample bottle was placed in the spectrophotometer sample slot, and the instrument was calibrated by pressing the "ZERO" button. The sample bottle was removed, the "Vario Sulpha 4/F10" reagent was added, tightly sealed, and inverted to ensure thorough mixing. This was followed by placing the bottle in the sample slot and pressing the "TEST" button. After the reaction occurred for 5 minutes, the measurement results were shown in mg/L.

2.2.1.7 Sodium Content Measurement

The measurement of sodium ions (Na^+) was carried out by comparing the difference between the total number of anions and cations. The results of anion and cation analyses in mg/L were converted to milliequivalents/L (mEq/L). The quantity of Na^+ was obtained by subtracting the total mEq of anions from the mEq of cations. Subsequently, the mEq/L value of Na^+ was converted to mg/L Na^+ by multiplication with the correction factor.

$$Ca^{2+}(ppm) = \frac{AxNx40,1x1000}{V} \quad \text{..... (1)}$$

$$Mg^{2+}(ppm) = \frac{(B-A)xNx24,3x1000}{V} \quad \text{..... (2)}$$

$$Cl^{-}(ppm) = \frac{(Vol\ titran)x(Ntitran)x35,450x1000}{V} \quad \text{..... (3)}$$

$$\text{barium content}\left(\frac{\text{mg}}{\text{L}}\right) = Cx\ fp \quad \text{..... (4)}$$

Explanation:
V = sample volume (mL)
N = normality of EDTA solution
A = volume of EDTA titrant required using murexide indicator
B = volume of EDTA titrant required using EBT indicator
C = concentration obtained from the measurement
fp = dilution factor

2.2.2 $CaCO_3$ Scale Dissolution Test

The scale sample used was 25 grams, with the volume of HCl solution, serving as scale dispersant, which varied at 0 mL, 10 mL, 20 mL, and 30 mL. Both components were placed in a container and soaked for 1 hour at room temperature. Subsequently, the solution was filtered to collect the undissolved scale sample. After drying, the sample was weighed, and the dispersed portion was calculated using the formula in Equation 5. The test was also conducted using a mixture of HCl solution (30 mL) and EDTA additive at concentrations of 0, 5, 10, 20, and 30 mL.

2.2.3 Corrosion Test

Approximately 25 grams of scale were weighed and placed into a test vessel using a holder containing 500 mL of dispersant solution, or approximately 2/3 of the test specimen volume. Scale dispersant solution consisted of EDTA solution with varying volumes ranging from 0 mL, 5 mL, 10 mL, 20 mL, and 30 mL, which was added to a 15% HCl solution, lasting for 24 hours. Subsequently, the test specimen was lifted, cleaned, and reweighed to determine the lost mass. The corrosion rate was calculated using Equation 6.

$$\%\ lost\ mass = \frac{(M0) - (M1)}{Mo}\ x\ 100 \quad \text{.....(5)}$$

$$corrosion\ rate = \frac{(Mo - M1)}{A\ x\ t\ x\ \rho} \quad \text{..... (6)}$$

Where:
M_0 = Initial mass
M_1 = Final mass
A = Surface area
t = Time
ρ = Density

3. Results and Discussion

3.1 Scale Identification

Scale is a solid compound originating from substantial amounts of ions present in water formation [19]. Furthermore, it disrupts the flow by reducing the inside diameter of the pipe which can hinder production and damage equipment [20].

Scale identification was conducted to understand the characteristics of scale formed inside the pipe. To measure scale growth, coupons are weighed by determining the increase in mass per unit of time. The component of water passing through the pipe generally affects scale formation, which is determined based on tests characterizing ions [8].

The results of formation water characteristics test in Table 1 showed the composition of ion content present in scale. The measurement results showed that the formation water has a pH of 7.34. This is because a higher pH increases the tendency for $CaCO_3$ scale formation. Based on the characteristic test, the formed scale was identified as carbonate, with a measured mass of 377.116 grams over 10 days.

Table 1. Identification test results

Parameter	mg/L	mEq/L
Ca^{2+}	236.472	11.600
Mg^{2+}	14.592	1.200
Ba^{2+}	-	-
Fe^{3+}	0.060	0.004
Na^{+}	7,828,309	340.406
Cl^{-}	11,458.187	322.794
HCO_3^{2-}	1,464.480	24.000
CO_3^{2-}	120.020	3.429
OH^{-}	0.000	0.000
SO_4^{2-}	163.000	3.187
pH	7.34	
scale mass	377.116 g	

3.2 Acidizing Treatment using HCl

The most commonly used acid to address the carbonate scale is HCl [16]. HCl is highly effective in dissolving carbonate scales as it reacts with carbonate formations, producing calcium chloride, carbon dioxide, and water [8]. The reaction that occurs is expressed as:

$$2HCl_{(aq)} + CO_3^{2-}{}_{(aq)} \longrightarrow 2Cl^-{}_{(aq)} + H_2O_{(l)} + CO_{2(g)}$$

Figure 2 shows that a 7.5% HCl solution with a volume of 5 mL can dissolve 36% of $CaCO_3$ scale. The solubility of scale continues to increase with the addition of HCl solution volume. This phenomenon occurs because higher acid concentrations result in more hydrogen ions in the solution, enhancing the ability of HCl to dissolve scale. Consequently, a 7.5% HCl solution with 10 mL and 20 mL volumes would dissolve 52% and 64% of scale, respectively. The highest dissolution capacity was achieved with a 7.5% HCl solution at a volume of 30 mL, dissolving 84% of $CaCO_3$ scale.

The test results using a 15% HCl solution in the acidizing treatment process are presented in Figure 2. It was discovered that 72% of $CaCO_3$ scale was dissolved in a 5 mL HCl solution. The use of a 15% HCl solution in the amount of 10 mL dissolves 80% of the scale. The solubility also increased with a higher volume of 15% HCl. The increase in the concentration of hydrogen ions in the solution affected the characteristics of the chemical reaction due to the high frequency of particle collisions [21]. Moreover, soluble complex compounds tend to form as the reaction balance shifts due to adding HCl.

The solubility of $CaCO_3$ scale reached 100% when using 15% HCl at volumes of 20 mL and 30 mL. Furthermore, it was discovered that the addition of acid could increase the porosity and permeability of the surface, resulting in easy solubility at high concentrations [22]. HCl solution demonstrated high effectiveness in removing $CaCO_3$ scale in acidizing treatment, with high dissolution power [23]. The comparison of the dissolution capabilities of 7.5% and 15% HCl solutions is shown in Figure 2. The results showed that higher concentration of HCl required a smaller volume for effective dissolution.

The results presented in Figure 2 showed that a 15% HCl solution in 20 mL and 30 mL volumes could remove 100% of the scale content within 60 minutes. The use of a 15% HCl solution in the amount of 30 mL showed a faster removal rate compared to a 20 mL solution, lasting for only 21 minutes. Consequently, the selected solution for the corrosion test was 15% HCl with a volume of 30 mL, which showed 100% performance dissolution in 21 minutes.

3.3 Acidizing Treatment using HCl and EDTA

Various acid compositions are commonly applied to enhance efficiency in acidizing treatment process [24]. Among several acid compositions, EDTA solution is a complex organic acid consisting of polycarboxylic amino acids that can be used as an additive.

Based on the test results shown in Table 2, higher content of EDTA additive in HCl solution resulted in a longer time required to dissolve scale. EDTA additive also formed complex bonds with metal ions, such as calcium-EDTA complex, which decelerated the dissolution process [25].

Previous research showed that the addition of EDTA to HCl solution could also act as an inhibitor, preventing scale formation on equipment [19]. Furthermore, the presence of additives acting as inhibitors can keep the cation-anion-forming scales in the solution [26]. For example, tartaric acid, when used as an additive, shows the ability to inhibit the growth of barium sulphate as the crystal structure formed causes difficulty in adhering to the equipment [6].

Based on the results of the 15% HCl and EDTA solution, corrosion rate was tested by adding EDTA solution with volumes of 0 mL, 5 mL, and 10 mL. This selection was influenced by the ability of the solution to achieve 100% performance in the dissolving scale at a relatively fast time, as shown in Table 2.

3.4 Measurement of Corrosion Rate

The speed of material quality deterioration over time can be expressed as a corrosion rate. The resistance level of material to corrosion generally has a corrosion rate value ranging from 1-200 mils per year (mpy) [27]. In this research, corrosion rate measurements using a 15% HCl solution, as shown in Figure 3, had a value of 186.255 mpy. Among the five levels of material resistance to corrosion, Mars G. Fontana (1987) in Afandi et al. [27] classified a range of 50-200 mpy in the poor corrosion resistance category, indicating a very high corrosion rate on the equipment. Generally, corrosion occurs in pipes due to a high acid concentration [1][28].

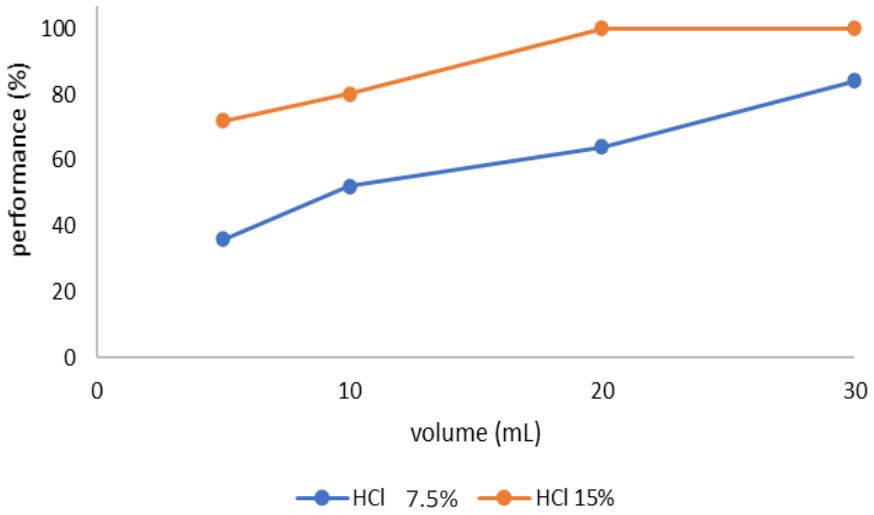

Figure 2. Scale solubility in HCl solution

Table 2. Test results of 15% HCl solution and EDTA additive

No	Solution Mix		$CaCO_3$ Scale			Total Time (minute)
	HCl 15% (mL)	EDTA (mL)	Initial Scale (g)	Final Scale (g)	Performance (%)	
1	30	0	25	0	100	21
2	30	5	25	0	100	30
3	30	10	25	0	100	33
4	30	20	25	0	100	39
5	30	30	25	0	100	46

Based on Figure 3, corrosion rate measurements for the mixture of 15% HCl and 5 mL EDTA showed a value of 46.754 mpy, belonging to the fair category. Meanwhile, the mixture of 15% HCl and 10 mL EDTA has a corrosion rate of 33.467 mpy, which categorizes it as corrosion-resistant (fair). The corrosion rate decreases by approximately 85% compared to the rate without using the EDTA additive.

The addition of EDTA additive in HCl solution reduced the corrosivity of HCl. This reduction was attributed to the numerous oxygen and nitrogen atoms in EDTA capable of binding with metal ions. EDTA additives can form complex compounds with metal ions in corrosion, specifically by binding with Ca^{2+}, Fe^{2+}, and Fe^{3+} ions [20].

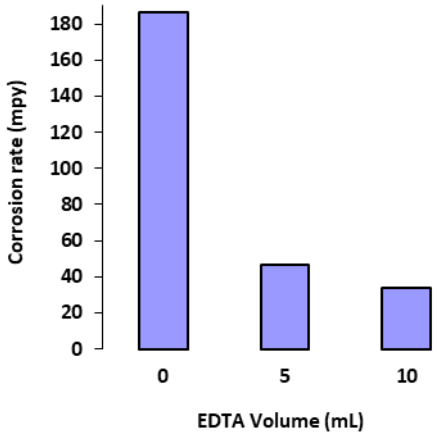

Figure 3. Corrosion rate measurement for a 15% HCl solution and EDTA addition

The research by Fouda et al. [29] showed that the addition of organic substances in HCl reduced the corrosion rate of zinc because the thin layer produced could isolate the metal surface. The use of oleic acid in the acidizing treatment process showed a decreased corrosion rate from 2,525.12 to 77.34 mpy [13]. The addition of other additives, such as arginine, to the HCl solution, also reduced the corrosion rate. This significant reduction occurred due to the function of arginine, acting as an inhibitor, and forming a passive layer on the surface, which obstructed the attack of corrosive solutions [14].

4. Conclusion

In conclusion, this research showed that acidizing treatment using a 15% HCl solution was highly effective in removing $CaCO_3$ scale. However, it had a corrosion rate of 186.255 mpy, which was categorized as poor. The addition of an EDTA additive solution at 10 mL in a 30 mL HCl solution in acidizing treatment method effectively eliminated the $CaCO_3$ scale and reduced the corrosion rate by 85%.

References

[1] Irawan, A., & Isjudarto, A. (2016). Evaluasi Penanggulangan Problem Scale Pada Flowline Sumur Tlj-Xxx Di Pt. Pertamina Ep Asset II Field Prabumulih Sumatera Selatan. *Teknik Pertambangan STTNAS Yogyakarta*, 1–6.

[2] Silva, C., Filho, D., Zanin, M., & Panossian, Z. (2021). Impact of Crude Oil Emulsion on Pipeline Corrosion. *Journal of Petrochemical Engineering*, 1(1), 11–19. doi: 10.36959/901/249

[3] Alighiri, D., Fatmala, C., Syafi, I., & Haditya, E. B. (2018). Studi Pembentukan Scale $CaCO_3$ dan $CaSO_4$ pada Air Formasi Sumur Minyak di Cepu, Indonesia. *Fisika*, 8(1), 28–36. doi: 10.15294/jf.v8i1.14496

[4] Ibrahim, P. A., & Fajri, A. N. (2020). Analisa Laju Pertumbuhan Silica Scaling pada Pipa Air Kondensat Scrubber Unit 5 di Industri Geothermal. *Molecules*, 2(1), 1–12. doi: 10.36418/jist.v1i4.42

[5] Musmuliadi. (2020). Scale Pada Pipa Produksi Area Minas Dengan Injeksi Chemical Scale Inhibitor, 7(1), 69–76. doi: 10.37859/jst.v7i1.2352

[6] Fatra, F., & Suwignyo, J. (2020). Analisa Pengaruh Penambahan Asam Tartrat Terhadap Pembentukan Kerak Di Dalam Pipa Pengeboran Minyak Bumi. *Journal of Automotive Technology Vocational Education*, 1(2), 1–8. doi: 10.31316/jatve.v1i2.991

[7] Septiani, M., Santoso, K., & Abdul Majid, R. (2019). Efektivitas Asam Nitrat (HNO_3) Sebagai Pelarut Alternatif Pada Proses Acid Wash Terhadap Plate Electrolyzer Di Pt Kaltim Nitrate Indonesia. *Journal of Chemical Process Engineering*, 3(2), 17. doi: 10.33536/jcpe.v3i2.258

[8] Kinasih, R. C., Amin, M., & Prabu, U. A. (2013). Analisa Hasil Acidizing Treatment untuk Menanggulangi Scale $CaCO_3$ dalam Upaya Mengoptimalkan Kemampuan Berproduksi Sumur R-11 PT. Pertamina EP Asset 2 Limau Field. *Journal of Earth Energy Engineering*, 7(April), 1.

[9] Gamal, H., Elkatatny, S., Al-Afnan, S., & Bahgat, M. (2021). Development of a Unique Organic Acid Solution for Removing Composite Field Scales. *ACS Omega*, 6(2), 1205–1215. doi: 10.1021/acsomega.0c04335

[10] Al-Shargabi, M., Davoodi, S., Wood, D. A., Ali, M., Rukavishnikov, V. S., & Minaev, K. M. (2022). A critical review of self-diverting acid treatments applied to carbonate oil and gas reservoirs. *Petroleum Science*. doi: https://doi.org/10.1016/j.petsci.2022.10.005

[11] Tian, Y., Guo, W., Wang, W., Wang, B., Zhang, P., & Zhao, T. (2023). Influence of organic corrosion inhibitors on steel corrosion in concrete under the coupled action of freeze–thaw cycles and chloride attack. *Construction and Building Materials*, 368, 130385. doi: 10.1016/j.conbuildmat.2023.130385

[12] Kahkesh, H., & Zargar, B. (2023). Estimating the anti-corrosive potency of 3-nitrophthalic acid as a novel and natural organic inhibitor on corrosion monitoring of mild steel in 1 M HCl solution. *Inorganic Chemistry Communications*, 158, 111533. doi: 10.1016/j.inoche.2023.111533

[13] Kementerian Energi dan Sumber Daya Mineral. (2020). *Sintesis Aditif Scale Removal Berbasis Asam Organik untuk Penanganan Scale Silika dan Karbonat Di Sumur Migas dan Panas Bumi*. Jakarta.

[14] Kayadoe, V. (2018). Kinerja arginin sebagai inhibitor korosi baja SS-304 dalam larutan HCl. *MjoCE*, 8(2), 103–112. doi: 10.30598/MJoCEvol8iss2pp103-112

[15] Bolzoni, F., Brenna, A., & Ormellese, M. (2022). Recent advances in the use of inhibitors to prevent chloride-induced corrosion in reinforced concrete. *Cement and Concrete Research*, 154, 106719. doi: https://doi.org/10.1016/j.cemconres.2022.106719

[16] Chacon, O. G., & Pournik, M. (2022). Matrix Acidizing in Carbonate Formations. *Processes*. doi: 10.3390/pr10010174

[17] Mohamed, A., Jr, D., & Bastidas, D. (2021). Significance of π–Electrons in the Design of Corrosion Inhibitors for Carbon Steel in Simulated Concrete Pore Solution. *Corrosion*, 77. doi: 10.5006/3844

[18] Liu, Z., Zhang, F., Li, X., & Wang, D. (2023). Improved corrosion inhibition of calcium disodium EDTA for mild steel in chloride-contaminated concrete pore solution. *Cement and Concrete Composites*, 140, 105075. doi: 10.1016/J.CEMCONCOMP.2023.105075

[19] Ahmad, N. M., & Said, L. (2015). Analisa Air Formasi dalam Menentukan Kecenderungan Pembentukan Scale pada Sumur X, Y dan Z. *Seminar Nasional Cendekiawan*, (ISSN: 2460-8696317), 317–325.

[20] Liestyana, R., & Said. (2018). Analisa Air Formasi terhadap Kecenderungan Pembentukan Scale Calcium Carbonat ($CaCO_3$) dan Calcium Sulfate ($CaSO_4$). *Prosiding Seminar Nasional Cendekiawan*, 0(0), 725–734. doi: 10.25105/semnas.v0i0.3528

[21] Norris, R., & Ryan, L. (2015). *Essential Chemistry for Cambridge IGCSE®*. OUP Oxford. Retrieved from https://books.google.co.id/books?id=xszKDwAAQBAJ

[22] Abdulraheem, A. (2022). Impact of HCl Acidizing Treatment on Mechanical Integrity of Carbonaceous Shale. *ACS Omega*, 7(16), 13629–13643. doi: 10.1021/acsomega.1c07175

[23] Jafarpour, H., Moghadasi, J., Khormali, A., Petrakov, D. G., & Ashena, R. (2019). Increasing

the stimulation efficiency of heterogeneous carbonate reservoirs by developing a multi-bached acid system. *Journal of Petroleum Science and Engineering*, 172, 50–59. doi: 10.1016/j.petrol.2018.09.034

[24] Xu, Z.-X., Li, S.-Y., Li, B.-F., Chen, D.-Q., Liu, Z.-Y., & Li, Z.-M. (2020). A review of development methods and EOR technologies for carbonate reservoirs. *Petroleum Science*, 17(4), 990–1013. doi: 10.1007/s12182-020-00467-5

[25] Wang, G., & Li, H. (2023). Metal extraction and analysis. In M. J. Goss & M. B. T.-E. of S. in the E. (Second E. Oliver (Eds.), (pp. 50–57). Oxford: Academic Press. doi: https://doi.org/10.1016/B978-0-12-822974-3.00144-0

[26] Raharjo, S. (2020). *Pembentukan dan Pengendalian Kerak Mineral di dalam Pipa*. Semarang, Jawa Tengah.

[27] Afandi, Y. K., Arief, I. S., & Amiadji. (2015). Analisa Laju Korosi pada Pelat Baja Karbon dengan Variasi Ketebalan Coating. *Institut Teknologi Sepuluh Nopember (ITS)*, 4(1), 1–5. doi: 10.12962/j23373539.v4i1.8931

[28] Nurfajri, I., Naubnome, V., & Hanifi, R. (2022). Pengaruh Variasi Presentase HCL Terhadap Laju Korosi, Nilai Kekerasan dan Struktur Mikro Sambungan Las TIG Baja ST 60. *Jurnal Ilmiah Wahana Pendidikan*, 8(19), 480–488. doi: 10.5281/zenodo.7222820

[29] Fouda, A. S., Rashwan, S., Emam, A., & El-Morsy, F. E. (2018). Corrosion Inhibition of Zinc in Acid Medium using some Novel Organic Compounds. *International Journal of Electrochemical Science*, 13(4), 3719–3744. doi: 10.20964/2018.04.23

CHEESA: Chemical Engineering Research Articles
ISSN **2614-8757 (Print)**, ISSN **2615-2347 (Online)**
Available online at: http://e-journal.unipma.ac.id/index.php/cheesa

Research Article

Optimization of Chromium (VI) Adsorption using Microalgae Biomass (*Spirulina sp.*) and its Application in Leather Tannery Waste

Optimasi Adsorpsi Kromium (VI) menggunakan Biomassa Mikroalga (Spirulina sp.) dan Aplikasinya pada Limbah Cair Penyamakan Kulit

Nais Pinta Adetya[1*)], Uma Fadzilia Arifin[2)], Emiliana Anggriyani[1)], Laili Rachmawati[1)]

1)Politeknik ATK Yogyakarta, Department of Leather Processing Technology, Indonesia
2)Politeknik ATK Yogyakarta, Department of Rubber and Plastic Processing Technology, Indonesia

Article History
Received: 09th May 2023; Revised: 12th December2023; Accepted: 02nd January 2024;
Available online: 22th January 2024; Published Regularly: December 2023

doi: 10.25273/cheesa.v6i2.16315.105-117

*Corresponding Author.
Email: naispinta26@gmail.com

Abstract

This study was conducted to examine the adsorption of Cr (VI) metal using Spirulina sp (inactive) biomass and its application in leather tannery wastewater. The treatment was carried out to determine the influence of independent variables on Cr (VI) adsorption with variations in pH, contact time, and metal solution concentration. The values of the solution pH, adsorption time, and concentration of the best metal solution were used to determine the center points of the optimization variables through Response Surface Methodology (RSM). The results showed that based on the FTIR test, macromolecules present in Spirulina sp biomass included amino, carboxylate, and hydroxy groups. The combination of factor variables that produced the optimum response was at pH 3.165, contact time of 66.58 minutes, and Cr (VI) metal ion solution concentration of 22.9 mg/L, resulting in a Cr (VI) adsorption efficiency of 69.66%. The adsorption pattern was included in the Freundlich adsorption isotherm, and the application of Spirulina sp biomass adsorbent to tannery waste reduced the concentration of Cr (VI) from 3.9 g/L to an undetectable level at <1.4 g/L.

Keywords: adsorption; chrome; microalgae; RSM; tanning

Abstrak

Penelitian ini bertujuan untuk mempelajari adsorpsi logam Cr (VI) menggunakan biomassa Spirulina sp. (inaktif) dan pengaplikasiannya pada limbah cair penyamakan kulit. Perlakuan penelitian dilakukan untuk mengetahui pengaruh variabel independen terhadap adsorpsi Cr (VI) dengan variasi pH, waktu kontak dan konsentrasi larutan logam. Hasil pH larutan, waktu adsorpsi dan konsentrasi larutan logam yang terbaik digunakan untuk penentuan titik-titik pusat variabel optimasi menggunakan Response Surface Methodology (RSM). Uji FTIR makromolekul penyusun biomassa Spirulina sp. mengandung gugus amino, karboksilat dan hidroksi. Kombinasi variabel faktor yang menghasilkan respon optimum berada pada pH 3,165, waktu kontak 66,58 menit, konsentrasi larutan ion logam Cr (VI) 22,9 mg/L dan menghasilkan respon efisiensi adsorpsi Cr (VI) sebesar 69,66%. Pola adsorpsi pada penelitian ini termasuk dalam isotherm adsorpsi Freundlich. Aplikasi adsorben biomassa Spirulina sp. pada limbah penyamakan kulit dapat menurunkan konsentrasi Cr (VI) dalam limbah yang awalnya sebesar 3,9 µg/L turun menjadi tidak terdeteksi (<1,4 µg/L).

***Kata kunci**: adsorpsi; krom; mikroalga; penyamakan; RSM*

1. Introduction

Liquid leather tannery waste is hazardous when directly disposed of into the environment due to its toxicity attributed to Cr (VI), sulfides, and ammonia content [1]. Cr (VI) is the most widely used tannery agent, accounting for approximately 85% of global leather tannery. The presence of heavy metals in water is absorbed and accumulated in the cells of organisms living in the environment [2].

Commonly used methods for waste treatment include precipitation, filtration, oxidation, ozonation, irradiation, ion exchange, or photodegradation. Adsorption is one highly efficient method for heavy metal removal from liquid waste [3].

Previous studies have used microalgae biomass in the absorption of heavy metal ions [4][5]. This study used *Spirulina sp.*, a type of microalgae, endemic to Indonesian waters and has a higher adsorption capacity compared to *Scenedesmus sp.* and *Oscillatoria sp.* in absorbing heavy metals from liquid waste [4][6].

Several microalgae species reportedly have the potential to absorb metal ions, either in the living (active) or dead (inactive) state [7]. Although *Spirulina sp.* has been used as an adsorbent for leather tannery waste through active culture for phytoremediation [8], the use of inactivated biomass remains unexplored. The use of inactive biomass is not dependent on the live cell metabolism, allowing for more flexibility in environmental conditions such as pH, light, and temperature. Optimization of the microalgae adsorption process for waste has also not been thoroughly examined. This step is necessary to obtain optimal variables in the adsorption process, and one method effective method is the Response Surface Methodology (RSM).

RSM is useful for optimizing processes, where the response obtained is influenced by independent variables [9]. This method is also used to establish a model depicting the relationship between independent variables and the response, showing the process conditions with the best response [10]. Therefore, this study aimed to determine the optimal pH, time, and concentration in the Cr (VI) adsorption process using *Spirulina sp.* biomass and its application to leather tannery waste.

2. Research Methods

2.1 Equipment and Materials

The materials used included *Spirulina platensis* biomass obtained from CV. Neoalgae (Sukoharjo, Central Java), chrome tannery process waste from a leather tannery industry in East Java, pure chromium standard solution with a concentration of 1000 mg/L from $K_2Cr_2O_7$ p.a 99.5% (Merck), HNO_3 (technical), and NH_4OH (technical).

The equipment used included a pH meter for pH control, a Fourier Transform Infrared (FTIR) Spectrophotometer for biomass functional group characterization, and an Ultraviolet-Visible (UV-Vis) Spectrophotometer for Cr (VI) concentration testing. The software used for Cr (VI) adsorption optimization was Statistica 10.

2.2 Adsorption Variable Influences

The independent variables were pH, time, and metal concentration, while biomass was mixed with Cr (VI) solution at specific concentrations and pH in Erlenmeyer flasks. This study used 0.1 M

HNO_3 and 0.1 M NH_4OH to adjust the solution pH. The metal solution concentrations were varied through dilution from a 1000 mg/L metal stock solution [11].

2.2.1 Influence of pH on adsorption

About 100 mL of Cr (VI) solution (20 mg/L) was prepared, and its pH was adjusted using 0.1 M HNO_3 and 0.1 M NH_4OH. The pH variations included 2, 3, 4, and 5, while 400 mg of biomass was added to each solution in a 250 ml Erlenmeyer flask. Stirring was carried out at room temperature using a magnetic stirrer for 60 minutes. The mixture was then filtered with Whatman 41 filter paper. The concentration of Cr (VI) ions after adsorption was determined with a UV-Vis spectrophotometer.

2.2.2 Influence of Contact Time on Adsorption

About 100 mL of Cr (VI) solution with a concentration of 20 mg/L at the optimum pH was mixed with 400 mg of biomass in a 250 mL Erlenmeyer flask and stirred at room temperature. Contact time was varied to 30, 60, 90, 120, 150, and 180 minutes, then the mixture was filtered with Whatman 41 filter paper, and the Cr (VI) concentration was determined using a UV-Vis spectrophotometer.

2.2.3 Influence of Solution Concentration on Adsorption

About 100 mL of metal solution with concentrations set at 10, 20, and 30 mg/L at optimum pH was mixed with 400 mg of biomass in a 250 mL Erlenmeyer flask at room temperature using the optimum time. Filtration was then performed, and the Cr (VI) concentration was determined with a UV-Vis spectrophotometer.

2.3 Determination of Adsorption Isotherms

Adsorption capacity and efficiency were calculated using Equations 1 and 2. The linear form of the Langmuir and Freundlich isotherm equations is shown in Equations 3 and 4.

$$q_e = \frac{(C_0 - C_e)V}{w} \quad \text{.....(1)}$$

$$\%E = \frac{(C_0 - C_e)}{C_0} x\ 100\ \% \text{.....(2)}$$

$$\frac{C_e}{q_e} = \frac{1}{Q_0 k_L} + \frac{C_e}{Q_0} \quad \text{.....(3)}$$

$$log(x/m) = \log k_F + \frac{1}{n}\log C_e \quad \text{.....(4)}$$

where, q_e is the adsorbed metal ion (mg/g); C_0 is the metal ion concentration before adsorption (mg/L); C_e is the metal ion concentration after adsorption (mg/L); V is the volume of the metal ion solution (L); w is the amount of *Spirulina sp.* biomass adsorbent (g) and %E is the adsorption efficiency. Q_o is the amount of adsorbed substance, and k_L is the Langmuir constant [11]. x is the amount of solute adsorbed. Meanwhile, m is the weight of the adsorbent used (g). k_F and n are constants that combine factors affecting adsorption, such as the capacity and intensity of adsorption [12].

2.4 Optimization of Cr (VI) Adsorption

Optimization aims to develop an empirical model to find optimal parameters for maximum or minimum responses [13]. This step can be performed using the RSM method [14]. The optimal pH of the solution, adsorption time, and metal solution concentration were determined to establish the central points of the variables. RSM was used to examine the influence of pH treatment, adsorption time, and metal solution concentration on the response variable, namely the adsorption efficiency of Cr (VI) metal ions.

Central Composite Design (CCD), an experimental design in RSM was used to construct a polynomial model of a mathematical function from independent variables to the response (y). The independent variables were pH (x_1), contact time (x_2), and Cr (VI) (x_3). The CCD experimental design was tabulated using Statistica 10 software. Based on the design type, 16 experiments are required, as summarized in Table 1.

The software analyzed the model that best fits the response conditions to identify the optimal points for the given response [15]. The lower, upper, and center points of the design were encoded as -1, 1, 0, and α, where +1 shows the high level, -1 the low level, $\alpha = 2^{n/4}$ (n is the number of variables or factors) represents the star point, and 0 signifies the center point. Star points were added to the design to generate an estimate of the surface area in the model, and the optimization formulation was presented in Table 2.

2.5 Application of Adsorption to Leather Tannery Waste

As part of the characterization stage, the waste was analyzed to determine the initial Cr (VI) concentration. The final Cr (VI) concentration in the waste was determined by adding 1 g of *Spirulina sp.* biomass adsorbent to 100 mL of waste at the optimum pH. Stirring was carried out at room temperature for the optimum time, followed by filtration. The filtrate was analyzed for Cr (VI) concentration as the final concentration in the waste. FTIR analysis was conducted for biomass characterization before and after Cr (VI) adsorption [11].

Table 1. CCD optimization

Run	x_1	x_2 (minute)	x_3 (mg/L)
1	2.00	30.00	10.00
2	2.00	30.00	30.00
3	2.00	90.00	10.00
4	2.00	90.00	30.00
5	4.00	30.00	10.00
6	4.00	30.00	30.00
7	4.00	90.00	10.00
8	4.00	90.00	30.00
9	3.00	60.00	20.00
10	1.24	60.00	20.00
11	4.76	60.00	20.00
12	3.00	7.08	20.00
13	3.00	112.9	20.00
14	3.00	60.00	2.36
15	3.00	60.00	37.64
16	3.00	60.00	20.00

Table 2. Optimization formula factors

Factor	Unit	Star Point (Low)	Low Level (-1)	Center point (0)	High Level (+1)	Star Point (High)
pH (x_1)		1.24	2.00	3.00	4.00	4.76
Contact time (x_2)	minute	7.08	30.00	60.00	90.00	112.91
Initial concentration of Cr (VI) (x_3)	mg/L	2.36	10.00	20.00	30.00	37.64

3. Results and Discussion

3.1 Characterization of Biomass with FTIR

FTIR results were used to identify functional groups in *Spirulina sp.* biomass. Based on the spectrum in Figure 1, *Spirulina sp.* biomass before Cr (VI) adsorption showed absorption at the wavenumber of 2928.57 cm^{-1} representing a stretching vibration of -OH [16]. There was also absorption at the wavenumbers of 3306 cm^{-1} and 1453 cm-1 showing stretching vibrations of N-H and C-H bonds respectively. Additionally, stretching vibrations of C=O (carboxylate ester) and C-O were observed at wavenumbers of 1652 cm-1 [17] and 1153 cm^{-1} [18]. FTIR results after Cr (VI) adsorption showed a shift in wavenumbers. Functional groups that experienced a shift in wavenumbers were assumed to play a role in Cr (VI) adsorption.

Adsorption of Cr (VI) metal resulted in a shift in wavenumbers due to the positively charged surface of the biomass, attracting anionic species electrostatically, and leading to strong physiosorption [19]. Therefore, based on the FTIR spectrum in Figure 1, functional groups in Spirulina sp. biomass implicated in the adsorption process of Cr (VI) included hydroxyl (-OH) from polysaccharides, C=O peptide (-CONH-) originating from proteins, and amine groups [5].

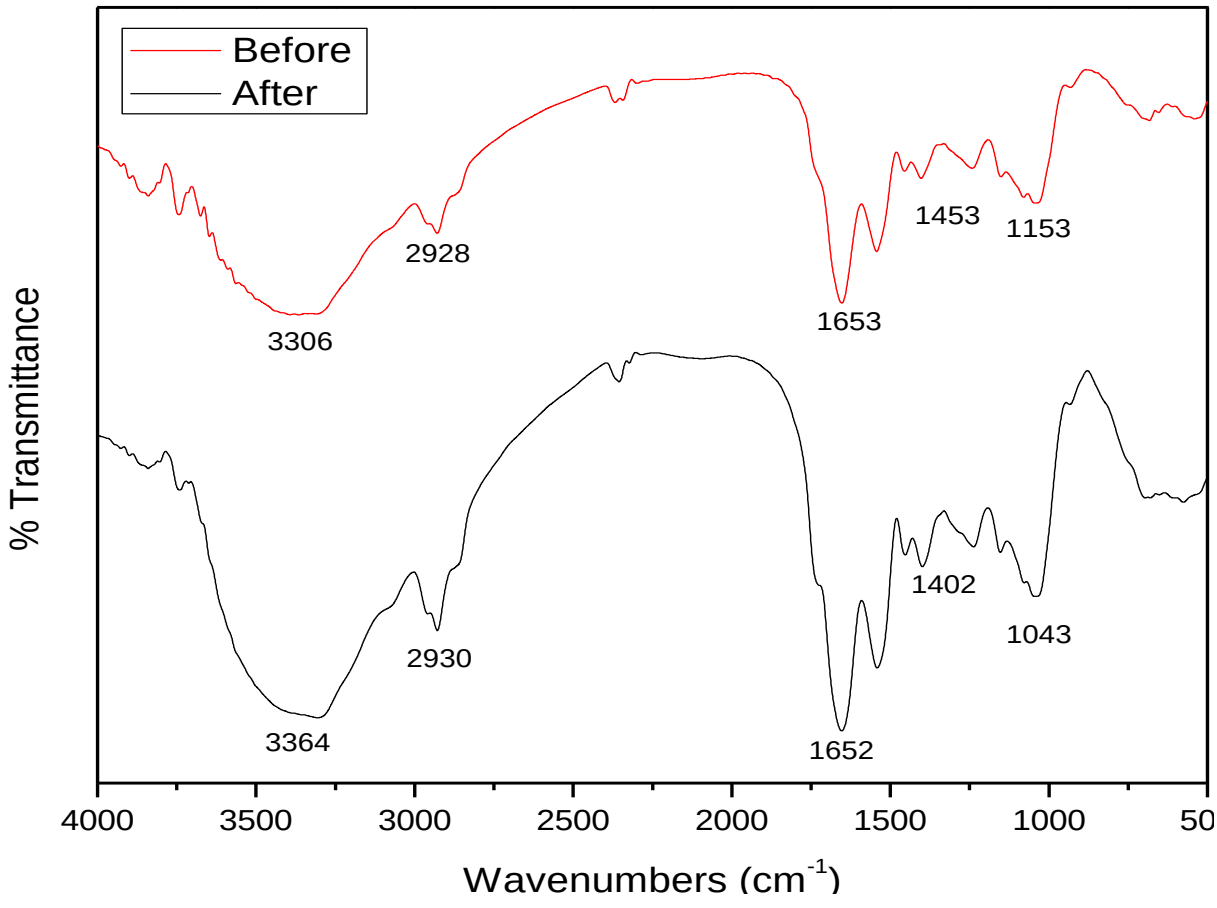

Figure 1. FTIR spectra of Spirulina biomass before and after Cr (VI) adsorption

3.2 Influence of pH on Adsorption

The initial pH of the solution is crucial for Cr (VI) adsorption because the protonation of the adsorbent configures active ion exchange sites and surface activity [20]. The results of Cr (VI) metal ion adsorption with pH variation are shown in Figure 2.

The highest adsorption capacity for Cr (VI) metal ions was achieved at an initial solution pH of 3. As discussed in the FTIR analysis, the biomass contains easily hydrolyzable groups including amines and aldehydes. Both of these groups are easily protonated, expanding more binding sites upon acidification of the biomass [4]. At low pH, the biomass surface containing anionic groups such as amines, carboxyls, and hydroxyls are protonated and become positively charged. Concurrently, through its free electron pairs, Cr (VI) metal ions in an acidic solution exist in the form of anionic species, such as $HCrO_4^-$, CrO_4^{2-}, and $Cr_2O_7^{2-}$, which easily interact with the adsorbent, resulting in a relatively high adsorbed amount.

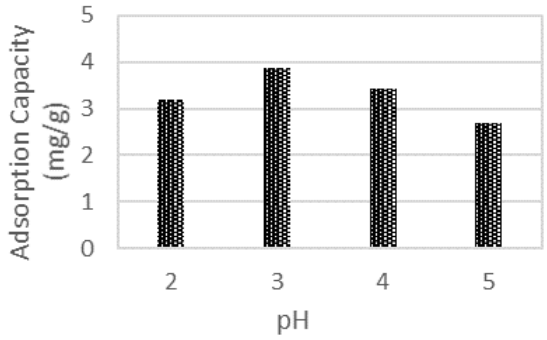

Figure 2. Influence of solution pH on Cr (VI) adsorption capacity

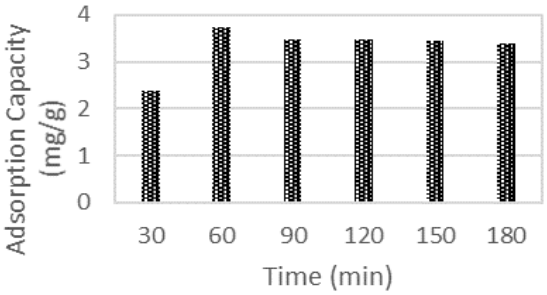

Figure 3. Influence of time on Cr (VI) adsorption capacity

3.3 Influence of Time on Adsorption

In the initial minutes (Figure 3), adsorption occurred rapidly due to the abundance of active sites in the adsorbent. However, after 60 minutes, Cr (VI) adsorption remained relatively constant. Extending the time up to 180 minutes did not significantly increase the adsorption capacity. Equilibrium was achieved at this point, where all active sites on the *Spirulina sp.* adsorbent were saturated. After reaching equilibrium, the significantly adsorbed amount of metal ions does not change with the additional contact time between Cr (VI) metal ions and the adsorbent [19].

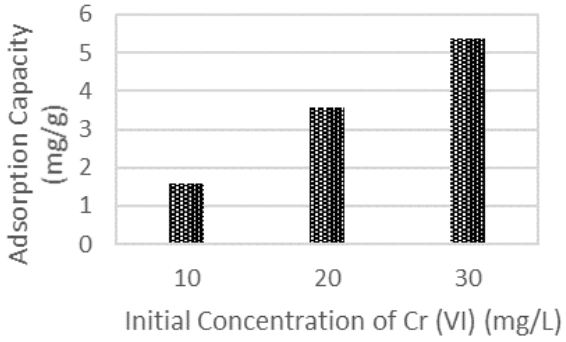

Figure 4. Influence of initial concentration of Cr (VI) on adsorption capacity

3.4 Influence of Cr (VI) Concentration on Adsorption

Based on Figure 4, the adsorption capacity of Cr (VI) was influenced by the metal concentration. In this case, increasing the concentration of the metal solution with a constant amount of adsorbent also improved the adsorption capacity. The number of active sites on the

adsorbent surface is proportional to the surface area [20]. When the active sites are not yet saturated, the increase in Cr (VI) concentration in contact will be proportional to heightened Cr (VI) adsorption capacity. The biomass surface has limited binding sites, and after completing adsorption at those sites, further loading of Cr is not feasible [5].

3.5 Adsorption Isotherm Model

The relationship between the adsorbate, adsorbent, and surface properties is reflected in the adsorption isotherm [21]. Adsorption data at various Cr (VI) concentrations were used to determine the adsorption isotherm.

Based on the R^2 value in Table 3, the Freundlich isotherm could better interpret the adsorption data (R^2 = 0.97) compared to the Langmuir isotherm, implying the adsorbent surface was heterogeneous [5]. Additionally, the adsorption observed followed a physisorption mechanism, causing weak bonding between the adsorbent and adsorbate, which allowed for desorption to occur, and the adsorbent could be reused [19].

Table 3 shows the parameter values in the adsorption isotherm, including k_F and 1/n values showing the capacity of the adsorbent, while k_F and Q_0 represent the maximum amount of adsorbate absorbed by the adsorbent in mg. The larger the k_F and Q_0 values, the greater the adsorption capacity. Based on this data, it was observed that the *Spirulina sp.* biomass adsorbent had a maximum adsorption capacity of 0.389 mg/g. The magnitude of 1/n provides a measure of adsorption favorability, with values between 1 and 10 showing favorable adsorption. For this study, the 1/n value also presents similar results, representing favorable adsorption [22].

3.6 Optimization of Factor Combinations for Cr (VI) Ion Adsorption

The central variable points were determined from the data on the best pH, time, and Cr (VI) concentration (Figure 3-4). Optimization of adsorption in this study used three independent variables, namely pH, time, and Cr (VI) concentration, as well as one response variable, the percentage of Cr (VI) adsorption. Optimal conditions were determined using Statistica 10 software to generate mathematical equations and polynomial models that fit the results [23].

The program determines the model type based on the coefficient of determination R^2 and the significance of the F_{count}. The type of polynomial model can also be observed from the sum of squares in the model order (Sequential Model Sum of Squares), lack of fit test, R^2, and adjusted-R^2 [24]. A model is considered good when it has significant values for the response and insignificant values for the lack of fit test. An insignificant lack of fit test value shows that the model is suitable or sufficiently represents the data [13].

Table 3. Langmuir and Freundlich isotherm parameters

Adsorbent	Freundlich Isotherm			Langmuir Isotherm		
	k_f (mg/g)	1/n	R^2	Q_0 (mg/g)	k_L (L/mg)	R^2
Spirulina sp. Biomass	0.21	1.43	0.97	7.54	0.41	0.58

The results obtained from 16 experiments are presented in Table 4. To find the predicted adsorption efficiency values, calculations were carried out based on the model equation determined according to the recommendations provided by STATISTICA 10, applying the CCD experimental design [25]. The model is presented in Equation 5, and the predicted flux values are depicted in Table 4.

$$y_{prediction} = 39.7290 + 18.1896x_1 + 0.9438x_2 + 4.1046x_3 - 2.2516x_1^2 - 0.0059x_2^2 - 0.0673x_3^2 - 0.1719x_1x_3 - 0.0072x_2x_3 \quad \text{.....(5)}$$

Description:
x_1 = pH of Cr (VI) metal ion solution
x_2 = contact time (minutes)
x_3 = concentration of Cr (VI) (mg/L)

Table 4 shows a difference between the observed and predicted values, as shown in the error column (% error). Therefore, a variance analysis was considered necessary to evaluate the suitability and accuracy of the experimental results obtained through an F-test. The accuracy test of the regression model was carried out by dividing the mean of squares of regression (MS_{reg}) and the mean of squares of residuals (MS_{res}). Both metrics were then compared with the table value of Fisher (F), where both M_{Sreg} and M_{Sres} represented the Sum of Squares divided by the Degree of Freedom [13]. The results of the subsequent variance analysis followed the hypotheses:
H_0 = all β_i values are zero
H_1= at least one β_i is not zero
H_0 is declared true if $F_{count}<F_{Table}$.

Another test was conducted to strengthen the assumption of model suitability through a lack of fit test [26], following the hypotheses:
H_0 = there is no lack of fit; the model created is suitable for the data
H_1 = there is a lack of fit; the model created does not represent the data

Table 4. Cr (VI) adsorption efficiency in 16 experiments

Run	pH	Time (minutes)	Concentration Cr (VI) (mg/L)	Adsorption Efficiency Cr (VI) (%)		
	x_1	x_2	x_3	$y_{observation}$	$y_{predictions}$	% error
1	2.00	30.00	10.00	40.78	39.41	3.33
2	2.00	30.00	30.00	56.31	56.49	0.32
3	2.00	90.00	10.00	48.78	49.60	1.66
4	2.00	90.00	30.00	56.03	58.06	3.62
5	4.00	30.00	10.00	47.72	45.34	4.99
6	4.00	30.00	30.00	56.71	55.54	2.04
7	4.00	90.00	10.00	56.06	55.52	0.94
8	4.00	90.00	30.00	56.10	57.11	1.80
9	3.00	60.00	20.00	68.67	66.38	3.32
10	1.24	60.00	20.00	58.30	57.18	1.92
11	4.76	60.00	20.00	60.01	61.58	2.62
12	3.00	7.08	20.00	42.31	44.81	5.91
13	3.00	112.91	20.00	57.23	55.17	3.58
14	3.00	60.00	2.36	35.43	37.22	5.05
15	3.00	60.00	37.64	55.02	53.68	2.43
16	3.00	60.00	20.00	64.05	66.38	3.64

H_0 was accepted when the p-value was more than the degree of significance, α = 0.05 [13]. The accuracy of this model was also reflected in the value of the coefficient of determination R^2. When the R^2 value exceeded 70%, it was considered accurate. This shows that the value estimated by the model is close to the experimental value. ANOVA calculations were obtained using STATISTICA Ver.10 Software as shown in Table 5.

Based on Table 5, the value of F_{Count} = 7.4775, while F_{Table} = 3.34. Given that F_{Count} was > F_{Table}, H0 was rejected and the alternative hypothesis H1 was accepted. In other words, the independent variables x_i had a significant influence on the model. Table 4 also shows that the p-value in the lack of fit test was 0.733, or greater than the α value. Therefore, H0 was accepted, signifying that the model was considered appropriate. The coefficient of determination, R^2, reached 0.96, hence, the model was considered suitable because it met the three test parameters [13].

The influences of each factor forming the equation were also analyzed based on the results of the ANOVA test. According to Equation 5, three effects influencing the value of Cr (VI) adsorption efficiency were observed, namely linear, quadratic, and interaction influences. An influence is considered statistically significant at $p \leq 0.05$. The impact of these three influences was determined by the coefficients, and the corresponding p-values were presented in Table 6.

Based on Table 6 and Equation 5, the variables pH, time, and the concentration of Cr (VI) metal ions, along with the quadratic influences, had a significant impact. All three variables showed a significant influence, both in terms of linear and quadratic. The quadratic factors of pH (x_1^2), adsorption time (x_2^2), and metal ion solution concentration (x_3^2) showed a negative impact on the response of adsorption efficiency. In contrast, the interaction between these factors had no significant influence on the adsorption efficiency of Cr (VI) because the p-values were greater than 0.05 [27]. Equation 5 was then simplified into Equation 6.

Table 6. Significance of each empirical model factor

Factor	p
x_1	0.020349
x_1^2	0.037510
x_2	0.001191
x_2^2	0.000795
x_3	0.000160
x_3^2	0.000211
$x_1.x_2$	0.999010
$x_1.x_3$	0.125761
$x_2.x_3$	0.067476

Table 5. Cr (VI) adsorption ANOVA

Source	Sum of squares	Degree of freedom	Mean square	F_{count}	$F_{0.05}$ (Table*)	p	R^2
SS regression	1330.368	9.00	147.8186	7.4775	3.34		0.9602
S.S. error	44.865	6.00	7.4775				
Lack of fit	34.193	5.00	6.8386			0.733	
S.S. total	1129.449						

*F_{Table} of F distribution percentages for 0.05% probability

y_{pred}= 39.7290 + 18.1896x_1 + 0.9438x_2 + 4.1046x_3 – 2.2516x_1^2 – 0.0059x_2^2 – 0.0673x_3^2 .....**(6)**

The optimum conditions were determined based on the stationary values for each model. Stationary values represent the highest response and serve as the best parameter for the performance of Cr (VI) metal ion adsorption. The position of the stationary point was identified mathematically using a matrix method assisted by STATISTICA Ver.10 software [28].

Optimization showed that the variables producing the optimum response for Cr (VI) adsorption efficiency at 69.66% were x_1=3.165, x_2=66.58 minutes, and x_3=22.90 mg/L. The RSM modeling results for Cr (VI) adsorption efficiency are illustrated in Figures 5 and 6 in the form of surface and contour plots. In this interaction, the initial concentration of Cr (VI) (x2) was set at 20 mg/L, which was the optimal initial concentration for Cr (VI) in the adsorption process.

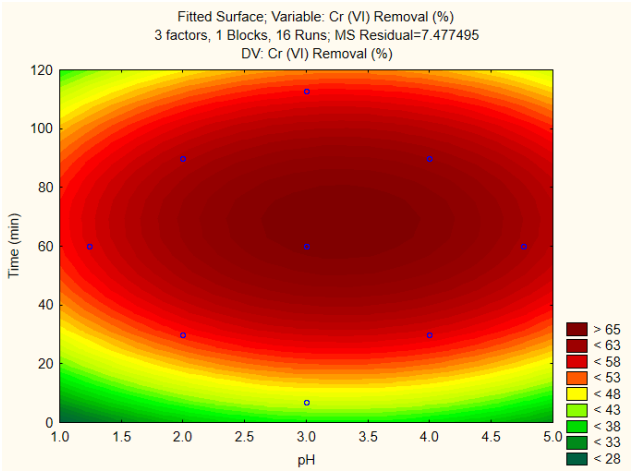

Figure 5. Contour plot of interaction of pH (x_1) with adsorption time (x_2) and initial concentration of Cr (VI) 20 mg/L (x_3) against percent adsorption of Cr (VI)

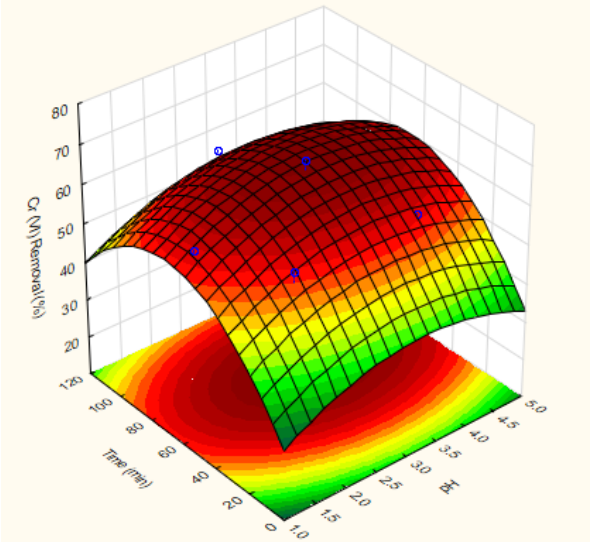

Figure 6. Surface plot 3D Interaction of pH (x_1) with adsorption time (x_2) and initial concentration of Cr (VI) 20 mg/L (x_3) on percent adsorption of Cr (VI)

The circular contour lines with a blue point at the center shown in Figure 5 depict the best response values, signifying an increase in the efficiency of Cr (VI) ion adsorption. The red-colored area represents the highest adsorption efficiency. The best response values were obtained by conditioning the factors at the central point, on the contour within the center of the circle. Figure 6 presents a three-dimensional representation of the adsorption efficiency response, showing that pH and time significantly influence the percentage removal of Cr (VI) with a maximum stationary region. The selection of codes representing data close to the optimum point (coded as 0) is crucial because a significant shift in prediction can result in the failure to find the optimum point [13].

Additional experiments under optimum conditions were conducted to confirm the predicted results. The optimization showed that the optimal adsorption conditions were x_1=3.165, x_2=66.58 minutes, and x_3 22.90 mg/L resulting in a Cr (VI) adsorption efficiency of 69.66%.

3.7 Application of Cr (VI) Adsorption on leather tannery waste

The initial concentration of Cr (VI) in tannery waste was 3.9 µg/L, and then adsorption was carried out using *Spirulina sp.* biomass adsorbent under known optimum conditions. Based on the test results, the Cr (VI) present in the wastewater sample after adsorption was undetectable (<1.4 µg/L). This shows that the use of *Spirulina sp*. biomass can reduce the Cr (VI) concentration in leather tanning wastewater. In another study that used Chlorella vulgaris microalgae biomass as an adsorbent for Cr (VI) in leather tanning wastewater, a reduction in Cr (VI) concentration reaching 30.01% was observed [29]. The decrease in efficiency observed was attributed to the significant interaction between the functional groups of microalgae biomass and other compounds (competitors) in wastewater during the chromium removal process [29].

4. Conclusion

In conclusion, *Spirulina sp.* biomass was identified as a suitable material for the adsorption of Cr (VI) from solutions. The functional groups detected in the composition included amino, carboxylate, and hydroxyl groups. Furthermore, the combination of factor variables that yielded the optimum response using the RSM method was at pH 3.165, contact time of 66.58 minutes, and concentration of Cr (VI) metal ion solution at 22.9 mg/L, resulting in an adsorption efficiency response of 69.66%. The application of *Spirulina sp.* biomass adsorbent in tannery wastewater effectively reduced the concentration of Cr (VI) from 3.9 µg/L to an undetectable level of <1.4 µg/L.

References

[1] Kuncoro, Y. M., & Soedjono, E. S. (2022). Studi Pustaka: Teknologi Pengolahan Air Limbah pada Industri Penyamakan Kulit. *Jurnal Teknik ITS*, 11(3). doi: 10.12962/j23373539.v11i3.99654

[2] Astuti, D., Sukmawati, N., Asyfiradayati, R., & Darnoto, S. (2022). Kajian Literatur Tentang Reduksi Kromium dalam Air Limbah Penyamakan Kulit dengan Fitoremediasi. *Syntax Literate ; Jurnal Ilmiah Indonesia*, 7(1), 146. doi: 10.36418/syntax-literate.v7i1.5723

[3] Endah, T., Buhani, & Suharso. (2015). Immobilization of cocodust biomass with silica gel as adsorbent for Cd (II) and Pb (II) ions in solution. In *Proceeding of the IConSSE FSM SWCU* (pp. 56–60).

[4] Pradhan, D., Sukla, L. B., Mishra, B. B., & Devi, N. (2019). Biosorption for removal of hexavalent chromium using microalgae Scenedesmus sp. *Journal of Cleaner Production*, 209, 617–629. doi: 10.1016/j.jclepro.2018.10.288

[5] Rezaei, H. (2016). Biosorption of chromium by using Spirulina sp. *Arabian Journal of Chemistry*, 9(6), 846–853. doi: 10.1016/j.arabjc.2013.11.008

[6] Katircioğlu, H., Aslim, B., & Tunçeli, A. (2012). Chromium (VI) biosorption from aqueous solutions by free and immobilized biomass of Oscillatoria sp. H1 isolated from freshwater. *ISIJ International*, 52(7), 1173–1178. doi: 10.2355/isijinternational.52.1173

[7] Gunasundari, & Kumar, S. (2017). Adsorption isotherm, kinetics, and thermodynamic analysis of Cu(II) ions onto the dried algal biomass (Spirulina platensis). *Journal of Industrial and Engineering Chemistry*, 56(Ii), 129–144. doi: 10.1016/j.jiec.2017.07.005

[8] Balaji, S., Kalaivani, T., Rajasekaran, C., Shalini, M., Vinodhini, S., Priyadharshini, S. S., & Vidya, A. G. (2015). Removal of heavy metals from tannery effluents of Ambur industrial area, Tamilnadu by Arthrospira (Spirulina) platensis. *Environmental Monitoring and Assessment*, 187(6), 1–10. doi: 10.1007/s10661-015-4440-7

[9] Radojkovic, M., Zekovic, Z., Jokic, S., & Vidovic, S. (2012). Determination of optimal extraction parameters of mulberry leaves using Response Surface Methodology (RSM) Received. *Romanian Biotechnological Letters*, 17(3), 7295–7308.

[10] Nurmiah, S., Syarief, R., Sukarno, S., Peranginangin, R., & Nurmata, B. (2013). Aplikasi Response Surface Methodology Pada Optimalisasi Kondisi Proses Pengolahan Alkali Treated Cottonii (ATC). *Jurnal Pascapanen dan Bioteknologi Kelautan dan Perikanan*, 8(1), 9. doi: 10.15578/jpbkp.v8i1.49

[11] Adetya, N. P., Arifin, U. F., & Anggriyani, E. (2021). The removal of chromium (VI) from tannery waste using Spirulina sp. immobilized silica gel. *Turkish Journal of Chemistry*, 45(6), 1854–1864. doi: 10.3906/kim-2106-22

[12] Hevira, L., & Gampito. (2022). The Kinetic Analysis and Adsorption Isotherm of Chicken Egg Shells and Membranes Against Synthetic Dyes. *Jurnal Riset Teknologi Pencegahan Pencemaran Industri*, 13(2), 28–36. doi: 10.21771/jrtppi.2022.v13.no2.p28-36

[13] Kusworo, T. D., Puji Utomo, D., Rahmatya Gerhana, A., & Angga Putra, H. (2018). Process Parameters Optimization in Membrane Fabrication for Produced Water Treatment Using Response Surface Methodology (RSM) and Central Composite Design (CCD). *Reaktor*, 18(1), 7. doi: 10.14710/reaktor.18.1.7-15

[14] Bayuo, J., Abukari, M. A., & Pelig-Ba, K. B. (2020). Optimization using central composite design (CCD) of response surface methodology (RSM) for biosorption of hexavalent chromium from aqueous media. *Applied Water Science*, 10(6), 1–12. doi: 10.1007/s13201-020-01213-3

[15] Nuvitasari, R., Rohman, A., & Martono, S. (2019). Response surface methodology used in the optimization of RP-HPLC condition for separation of carmine and rhodamine B. *Indonesian Journal of Pharmacy*, 30(4), 276–284. doi: 10.14499/indonesianjpharm30iss4pp276

[16] Tavares, L., & Noreña, C. P. Z. (2021). Characterization of the physicochemical, structural, and thermodynamic properties of encapsulated garlic extract in multilayer wall materials. *Powder Technology*, 378, 388–399. doi: 10.1016/j.powtec.2020.10.009

[17] Tao, Y., Wu, Y., Yang, J., Jiang, N., Wang, Q., Chu, D. T., … Zhou, J. (2018). Thermodynamic sorption properties, water plasticizing effect, and particle characteristics of blueberry powders produced from juices, fruits, and pomaces. *Powder Technology*, 323, 208–218. doi: 10.1016/j.powtec.2017.09.033

[18] Mokone, J. G., Tutu, H., Chimuka, L., & Cukrowska, E. M. (2018). Optimization and Characterization of Cladophora sp. Alga Immobilized in Alginate Beads and Silica Gel for the Biosorption of Mercury from Aqueous Solutions. *Water, Air, and Soil Pollution*, 229(7). doi: 10.1007/s11270-018-3859-1

[19] Sathvika, T., Manasi, Rajesh, V., & Rajesh, N. (2016). Adsorption of chromium supported with

various column modeling studies through the synergistic influence of Aspergillus and cellulose. *Journal of Environmental Chemical Engineering*, 4(3), 3193–3204. doi: 10.1016/j.jece.2016.06.027

[20] Sibi, G. (2016). Biosorption of chromium from electroplating and galvanizing industrial effluents under extreme conditions using Chlorella vulgaris. *Green Energy and Environment*, 1(2), 172–177. doi: 10.1016/j.gee.2016.08.002

[21] Li, Q., Huang, Q., Pan, X. Y., Yu, H., & Zhao, Z. T. (2022). Adsorption behavior of Cr(VI) by biomass-based adsorbent functionalized with deep eutectic solvents (DESs). *BMC Chemistry*, 16(1), 1–14. doi: 10.1186/s13065-022-00834-w

[22] Kumar, M., Singh, A. K., & Sikandar, M. (2020). Biosorption of Hg (II) from aqueous solution using algal biomass: kinetics and isotherm studies. *Heliyon*, 6(1), 1–32. doi: 10.1016/j.heliyon.2020.e03321

[23] Dakhil, I. H., Naser, G. F., & Ali, A. H. (2021). Response Surface Modeling of Arsenic Adsorption by Modified Spent Tea Leaves. *IOP Conference Series: Materials Science and Engineering*, 1090(1), 012129. doi: 10.1088/1757-899x/1090/1/012129

[24] De Schepper, W., Vanschepdael, C., Huynh, H., & Helsen, J. (2020). Membrane capacitive deionization for cooling water intake reduction in thermal power plants: Lab to pilot scale evaluation. *Energies*, 13(6). doi: 10.3390/en13061305

[25] El-Mekkawi, S. A., Abdelghaffar, R. A., Abdelghaffar, F., & El-Enin, S. A. A. (2021). Application of response surface methodology for color removal from dyeing effluent using de-oiled activated algal biomass. *Bulletin of the National Research Centre*, 45(1). doi: 10.1186/s42269-021-00542-w

[26] Ahmad, S., Pathak, V. V., Kothari, R., Kumar, A., & Naidu Krishna, S. B. (2018). Optimization of nutrient stress using C. pyrenoidosa for lipid and biodiesel production in integration with remediation in dairy industry wastewater using response surface methodology. *3 Biotech*, 8(8), 0. doi: 10.1007/s13205-018-1342-8

[27] Iqbal, M., Iqbal, N., Bhatti, I. A., Ahmad, N., & Zahid, M. (2016). Response surface methodology application in optimization of cadmium adsorption by shoe waste: A good option of waste mitigation by waste. *Ecological Engineering*, 88, 265–275. doi: 10.1016/j.ecoleng.2015.12.041

[28] Hadiyanto, S. H. (2016). Response surface optimization of ultrasound-assisted extraction (UAE) of phycocyanin from microalgae Spirulina platensis. *Emirates Journal of Food and Agriculture*, 28(4), 227–234. doi: 10.9755/ejfa.2015-05-193

[29] Ardila, L., Godoy, R., & Montenegro, L. (2017). Sorption Capacity Measurement of Chlorella Vulgaris and Scenedesmus Acutus to Remove Chromium from Tannery Waste Water. *IOP Conference Series: Earth and Environmental Science*, 83(1). doi: 10.1088/1755-1315/83/1/012031

CHEESA: Chemical Engineering Research Articles
ISSN **2614-8757 (Print)**, ISSN **2615-2347 (Online)**
Available online at: http://e-journal.unipma.ac.id/index.php/cheesa

Research Article

Optimization and Characterization of Adsorbent from Palm Kernel Shell Waste Using H_3PO_4 Activator

Optimasi dan Karakterisasi Adsorben dari Limbah Cangkang Kelapa Sawit Menggunakan Aktivator H_3PO_4

M. Julian Herlambang[1)], Adityas Agung Ramandani[2)], Devy Cendekia[1*)], Livia Rhea Alvita[1)], Yeni Ria Wulandari[1)], Shintawati[1)], Mawar Siti Purnani[1)], Dimas Amirul Mukminin Nur Efendi[1)]

[1)]Politeknik Negeri Lampung, Teknologi Rekayasa Kimia Industri, Indonesia
[2)]Yuan Ze University, Chemical Engineering and Materials Science, Taiwan

Article History
Received: 09th Maret 2023; Revised: 27th November 2023; Accepted: 02nd January 2024; Available online: 13th February 2024; Published Regularly: December 2023

doi: 10.25273/cheesa.v6i2.15906.118-125

*Corresponding Author.
Email:
devycendekia@polinela.ac.id

Abstract

Palm kernel shell is solid waste produced from the processing of crude palm oil (CPO). In this context, phosphoric acid (H_3PO_4) serves as an essential activator for producing an adsorbent with maximum micropore under operating conditions at a temperature of <450°C. Therefore, this study aimed to determine the optimal adsorbent condition of the palm kernel shell using H_3PO_4 activator. The production process was optimized using Response Surface Methodology (RSM) and Central Composite Design (CCD) methods with activator concentration variations of 4%, 5%, and 6%, at activation times of 23 hours, 24 hours, and 25 hours, respectively. The quality of the adsorbent produced fulfilled SNI standard 06-3730-1995, characterized by water content of 1.001%, ash content of 5.767%, missing substance level of 18.932%, and fixed carbon content of 75.301%. Furthermore, this work effectively optimized the RSM and CCD adsorbent production process, achieving 4.785% variation in activator concentration and 24.679 hours activation time.

Keywords: adsorbent; fixed carbon; H_3PO_4 activator; iodine charcoal power; palm kernel shell

Abstrak

Cangkang kelapa sawit adalah salah satu limbah padat yang dihasilkan dari proses pengolahan minyak kelapa sawit. Aktivator H_3PO_4 dapat menghasilkan adsorben yang memiliki mikropori maksimum pada kondisi operasi suhu <450 °C. Tujuan penelitian ini adalah untuk menentukan kondisi optimum adsorben dari cangkang kelapa sawit dengan menggunakan aktivator H_3PO_4. Proses pembuatan adsorben dioptimasi menggunakan metode Response Surface Methodology (RSM) khususnya Central Composite Design (CCD) dengan variasi konsentrasi aktivator yaitu 4%, 5%, dan 6% serta dengan variasi waktu aktivasi yaitu 23 jam, 24 jam, dan 25 jam. Kualitas adsorben dari cangkang kelapa sawit telah sesuai dengan standar SNI 06-3730-1995 pada karakteristik kadar air 1,001%, kadar abu 5,767%, kadar zat yang hilang 18,932%, fixed carbon 75,301%. Selain itu, penelitian ini juga berhasil mengoptimalkan proses pembuatan adsorben menggunakan metode RSM dan CCD dengan variasi konsentrasi aktivator 4,785% dan waktu aktivasi selama 24,679 jam.

***Kata kunci**: adsorben; aktivator H_3PO_4; cangkang kelapa sawit; daya jerap iod; fixed carbon*

1. Introduction

In Indonesia, the palm oil mill industry is experiencing significant growth, with an annual production of two million tons [1]. This phenomenon has led to the generation of a substantial amount of waste, requiring the adoption of net zero waste and the development of treatment initiatives to prevent greenhouse gas emissions. According to the 2020 data from the National Statistical Agency, Indonesia has 14,858,000 hectares of palm plantations, with 196,000 hectares located in Lampung Province [2].

The primary products of palm industry are liquid and solid waste, as well as crude palm oil (CPO). This solid waste comprises the palm kernel shell, the empty bunch, and the sludge from the decanter's output. Meanwhile, liquid waste consists of the exhaust waste from the sterilization and clarifier stations. Solid waste is considered suitable for processing into valuable products such as plant fertilizer made from sludge and empty palm [3]. However, palm kernel shell waste has not been fully exploited for large-scale use due to its harder texture, and application as fuel for boilers. In industry settings, the exploitation is against the existing rules, causing damage to boiler pipes.

Palm kernel shell constitutes approximately 60% of waste generated in the production of palm oil. Furthermore, it consists of hemicellulose, cellulose, lignin, and ashes, with a proportion of 33.52%, 38.52%, 20.36%, and 3.92%, respectively [4]. To mitigate the environmental impact of this waste, using palm kernel shell as an adsorbent offers a promising solution. The resultant adsorbent produced in this method can be used to remove hazardous chemicals or heavy metals from wastewater, contributing to the reduction of air and water pollution.

Adsorbent technique uses chemical processes to remove heavy metals, while aeration and biosorbent cellulose xanthate demand more energy [6,7]. Therefore, to address heavy metals related to water and air pollution, absorbent method is a cost-effective and environmentally responsible substitute.

A previous study conducted by Hendra reported that the highest quality absorbent could be made from palm kernel shell at a temperature of 850^oC [8]. In order to increase the adsorbent's adsorption capacities and efficiency, chemicals including phosphate acid (H_3PO_4) [9], chloric acid (HCl) [10], sodium hydroxide (NaOH), and potassium hydrogen oxide (KOH) [11] have also been used in the activation process. Specifically, H_3PO_4 activator has shown the ability to effectively produce chemical reactions in the synthesis of organic compounds [12], increasing final product yield to ensure better adsorption with enhanced physical and chemical stability. This makes adsorbent suitable for use in gas filters, water purification, catalyst supports, and the treatment of industrial waste [13-15]. Therefore, this study aimed to determine the optimal conditions for converting palm kernel shell into adsorbent using H_3PO_4 activator.

2. Research Methods

This study was conducted at the Analysis and Chemical Industry Laboratory of the Politeknik Negeri Lampung on March 29th and October 31st, 2022. The ingredients used included palm kernel shell, H_3PO_4 solution (Merck), iodine (Merck), starch 1%, KIO_3 (Merck), sodium thiosulfate 0.1 N, and aquadest.

Furthermore, the tools used included laboratory pyrolysis, a drying oven (UN 110, Memmert, German), an analytical balance (Shimadzu, Japan), a pH meter, a furnace, thermometer, and a grinder.

2.1 Collection, preparation, and activation using H_3PO_4

Palm kernel shell was collected from PT Anaktuha Sawit Mandiri, Wates, Lampung Tengah, Indonesia. A pyrolysis process, as shown in Figure 1 was used to burn 500 g palm kernel shell at a temperature of 400 ^oC for 4 hours [16-18]. Subsequently, a pyrolysis coal was put into the grinder machine to reduce the size to 100 mesh. Charcoal powder was stored at room temperature of 25 ^oC, preventing water absorption. The activation with H_3PO_4 was carried out as an adsorbent to enhance adsorption capabilities. Response Surface Methodology (RSM) was used for the combination of adsorbent production from palm kernel shell, as shown in Table 1.

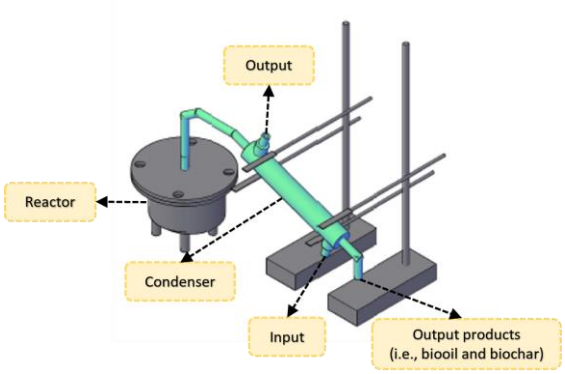

Figure 1. Pyrolysis laboratory-scale for burning kernel shell.

Each 100 g of charcoal powder was activated using three different concentrations: 4%, 5%, and 6% [19]. The activation was carried out at different times, including 23, 24, and 25 hours. After activation, distilled water was used to filter and neutralize adsorbent to a pH of 7, which was placed into the oven to dry at 110°C for 3 hours. Product adsorbent was carried out to determine optimum conditions during activation using H_3PO_4 and activation time.

Tabel 1. Experimental design of adsorbent production

Run-n	Concentration activator (%)	Activation time (Hours)
1.	4	23
2.	4	24
3.	4	25
4.	5	23
5.	5	24
6.	5	24
7.	5	24
8.	5	24
9.	5	24
10.	5	25
11.	6	23
12.	6	24
13.	6	25

2.2 Adsorbent Characterization

The characterization of adsorbent was based on SNI 06-3730-1995, such as water, ash, and lost substance content, including fixed carbon, and iodine adsorption capacity. These parameters were measured to determine the quality and effectiveness of adsorbent. Subsequently, the optimum conditions were determined using RSM with Central Composite Design (CCD) model in the Design Expert version 13 software [20].

2.2.1 Quantification of water content

An adsorbent weighing 0.5 g was inserted into the cup, and it was baked for 3 hours at 115 ^oC. Subsequently, the cup was inserted in the desiccator for 10 minutes, weighed using an analytical balance, and counted with Equation 1 to

determine the final weight. Where, a, b, and c (gram) indicated empty cup, empty cup and initial sample, as well as weight cup and sample after the oven, respectively.

$$Water\ content\ (\%) = \frac{(b-c)}{(b-a)} \times 100\% \quad \textbf{.....(1)}$$

2.2.2 Quantification of ash content

Weighed at 1 g, the adsorbent was placed in an empty cup and heated to 900 ^oC for two hours in a furnace. The cup was inserted in the desiccator for 10 minutes, weighed using an analytical balance, and counted with Equation 2 to determine the final weight. Where, a, b, and c (gram) indicated empty cup, empty cup and initial sample, as well as weight cup and sample after the furnace, respectively.

$$Ash\ content\ (\%) = \frac{(c-a)}{(b-a)} \times 100\% \quad \textbf{.....(2)}$$

2.2.3 Quantification of lost substance content

Approximately 1 g of adsorbent was weighed, put into an empty cup, placed into a furnace at a temperature of 950^oC for 15 minutes, and inserted into the desiccator for 10 minutes. Subsequently, the cup was weighed using an analytical balance and counted with Equation 3 to determine the final weight. Where, a and b (g) indicated empty cup and initial sample as well as weight cup and sample after the furnace, respectively.

$$Weight\ loss\ (\%) = \frac{(a-b)}{a} \times 100\% \quad \textbf{.....(3)}$$

2.4.4 Quantification of fixed carbon (FC)

FC was determined using Equation 4 following adsorbent removal of water, ash, and lost substance content. Where A, B, and C presented water content, ash content, and weight loss, respectively.

$$FC\ (\%) = 100\% - \big(A + B + (A - C)\big) \quad \textbf{.....(4)}$$

2.4.5 Quantification of iodine adsorption

A 0.5 g adsorbent was added to 5 mL of 0.1 N Iodine solution and infused for 15 minutes. The solution was added to 25 mL of aquadest, and 5 mL filtrate was irrigated with a 0.1 N sodium thiosulfate solution until the yellow disappeared. This was followed by the addition of 1% amino solution and titration again until the blue color became uncolored. Subsequently, the power of iodine adsorption was calculated using Equation 5. Where, W, V_1, V_2, N_1, and N_2 represent of mass of adsorbent, filtrate volume, titrate volume, concentration of $Na_2S_2O_3$, and Iodium, respectively.

$$Iod\ (mg/g) = \frac{(V_1 - V_2) \times N_1 \times N_2}{W} \times 126.93 \quad \textbf{.(5)}$$

3. Results and Discussion

Table 2 shows the characterization results of adsorbent generated, including the quantities of water, ash, substance loss, fixed carbon, and iodine resin capacity.

3.1 Water content of adsorbent

Table 2 shows the highest water content of 1.0037%, with a combination of activator concentrations and activation times of 4% and 25 hours, respectively. The lowest water content of 1.000% was found at activator concentration of 4% and an activation time of 23 hours. Another study stated that water content obtained

from palm kernel shells with the H_3PO_4 activator was 5.30% [21]. In this context, palm kernel shell adsorbent performed better compared to cocoa shell. An excessive amount of water in the adsorbent would disrupt the adsorption process, as the molecule or particle dissolved in water and became ineffective at interacting with the surface [22]. This disruption can reduce the efficiency of the absorption process and desired final result.

The airborne residue yield that was obtained complied with SNI 06-3730-1995, at approximately 15%. This suggested that the resulting adsorbent had a longer shelf life. Furthermore, the similarity of the free variables employed in the experiment may have contributed to the low water content, which averaged 1%.

3.2 Ash content of adsorbent

In the treatment with a 4% activator concentration over 23 hours of activation, the maximum adsorbent ash level was found to be 8.32%. Furthermore, there was a low ash level of 3.22% at a 6% activator concentration for 25 hours. The resulting palm kernel shell adsorbent had an ash content of less than 10%, based on SNI 06-3730-1995.

A previous study conducted by Syamsudin reported that an increase in ash levels could occur due to the formation of mineral salts during the carbonization process [23]. When the carbonization process was excessively long at a higher temperature, a significant increase would be anticipated in the ash level on the adsorbent.

Table 2. Results of characterizing adsorbent from palm kernel shell with H_3PO_4 activator

Run-n	Water content (%)	Ash content (%)	Substance loss (%)	Fixed carbon (%)	Iodine Adsorption ($mg.g^{-1}$)
1.	1.0002	8.32	20.82	70.86	603.10
2.	1.0005	7.93	20.56	71.50	610.56
3.	1.0037	6.33	19.88	73.79	595.89
4.	1.0002	5.72	18.84	75.44	620.34
5.	1.0006	5.75	18.51	75.74	636.92
6.	1.0007	5.77	18.53	75.70	626.66
7.	1.0005	5.79	18.54	75.67	625.53
8.	1.0006	5.78	18.44	75.78	646.91
9.	1.0008	5.73	18.52	75.75	640.19
10.	1.0032	5.36	18.45	76.19	640.09
11.	1.0004	4.16	17.32	78.52	707.14
12.	1.0006	3.91	17.10	78.99	709.25
13.	1.0007	3.22	17.04	79.74	703.62
SNI 06-3730-1995	Max. 15	Max. 10	Max. 25	Min. 65	Min. 750

3.3 Lost substances in palm kernel shell

The most lost substance test results were obtained at a 23-hour activation time of 20.82% and a 4% activator concentration. With an activator concentration of 6% and an activation time of 25 hours, 17.04% of adsorbent had the lowest amount of lost substances. This showed that the adsorbent level of lost substance at 950^{o}C heating was less than 25%, in compliance with SNI 06-3730-1995, allowing its use as an adsorbing agent. In this study, pyrolysis was used to carbonize palm kernel shell, at a

temperature of 400°C for 4 hours [24,25]. This investigation also showed that the amount of lost substance increased when carbonization was carried out at low temperatures for a short period of time.

3.4 Fixed carbon

The highest fixed carbon result of 78.99% was obtained at 6% activator concentration and a 24-hour activation time. Meanwhile, the lowest fixed carbon result at 4% concentration was obtained at 23 hours of activation, with 70.86%. Activator concentration and activation time had an impact on the value of the fixed carbon rate generated. In adsorption process, high fixed carbon levels are preferable to low, as adsorbents perform better when the pore surfaces are larger [24]. Fixed carbon from adsorbent produced complied with SNI 06-3730-1995, which was at least 65%. This compliance enables fixed carbon to be used as an adsorbent to remove water-soluble substances such as heavy metals and organic materials. Additionally, high capacity of adsorbent facilitated the effective absorption of substances.

3.4 Iodine adsorption power

The highest-performing iodine cranes of 709.25 mg/g were generated at a 24-hour activation time and activator concentration of 6%. The lowest iodine potency was found at a 4% activator concentration and a 23 hours activation time of 603.10 mg/g. However, the SNI 06-3730-1995 requirement for technical activated carbon of 750 mg/g was not met by adsorbent made using iodine cranes. This phenomenon occurred due to the prolonged exposure of iodine solution to sunlight during the titration procedure, causing variation in concentration. Moreover, the ability of the adsorbent to adsorb iodine indicates deactivation, due to an increase in adsorption power [26].

3.5 Optimization of adsorbent production

In this study, Design Expert Version 13 software was used in the optimization to determine the ideal threshold for activator consistency and activation time during the adhesive manufacturing process. The ideal activator coefficient and activation time of 4.785% and 24.679 minutes, respectively, were used to determine the desirability coefficient of 1, as shown in Figure 2.

Figure 2 shows optimization results using desirability values, considering the activator concentration and activation time simultaneously. The selection of desirability values in the optimization process is essential, as a lower value (<1) results in reduced accuracy.

4. Conclusion

In conclusion, this study showed that the ideal conditions for producing adsorbent were 4.785% concentration and 24.679 hours activation time in H_3PO_4 activator. The amount of iodine charcoal produced increased with the concentration of activator used. The Water content of adsorbent obtained under ideal conditions was 1.001%, followed by ash, lost substance, and fixed carbon content of 5.767%, 18.932%, and 75.301%, respectively, according to SNI 06-3730-1995. However, the iodine resin capacity that was produced did not meet the 619.866 mg/g SNI standard.

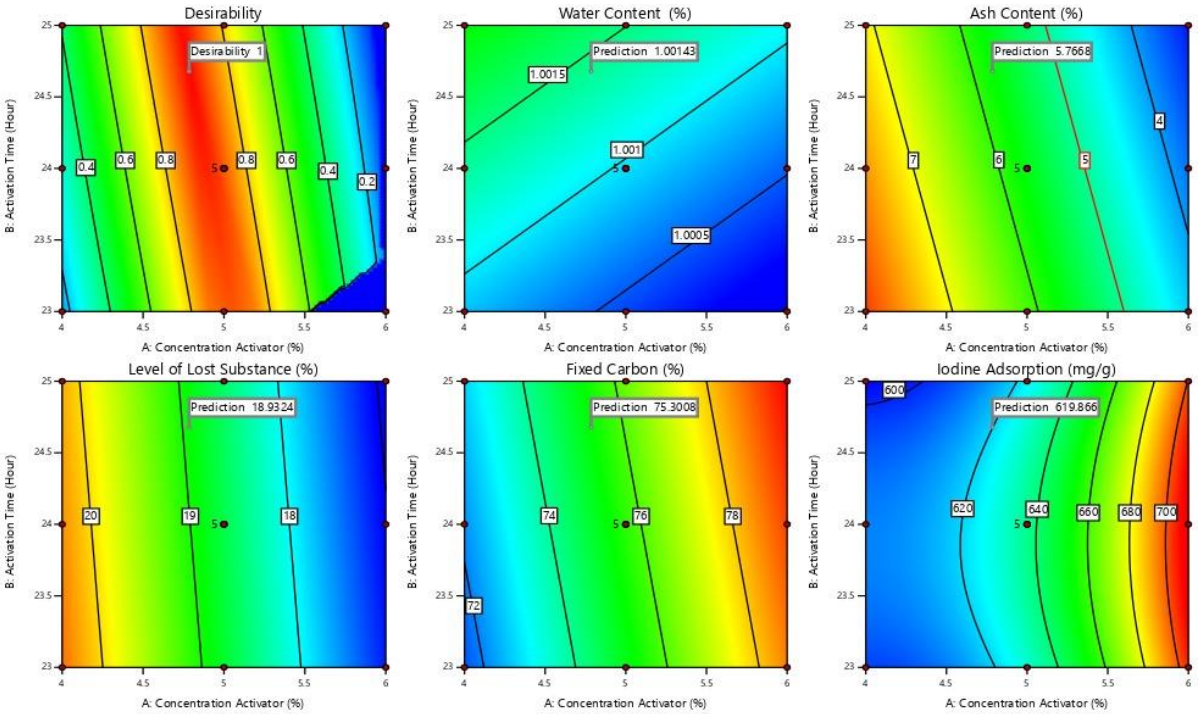

Figure 2. Design Expert for optimizing palm kernel shell adsorbent

References

[1] Fauziah, N. (2009). Pembuatan Arang Aktif Secara Langsung dari Kulit Acacia mangium Wild Dengan Aktivasi Fisika dan Aplikasinya Sebagai Adsorben. *Skripsi*, Dep. Hasil Hutan, IPB.

[2] BPS, *Stastika Kelapa Sawit Indonesia*. (2020), 1-9. Retrieved from https://www.bps.go.id/id/publication/2021/11/30.

[3] Muhammad H. J., Dadan Permana. (2014). Pemanfaatan Tandan Kosong Sawit Untuk Pupuk Organik Pada Intercropping Kelapa Sawit Dan Jagung. *Jurnal Pengkajian dan Pengembangan Teknologi Pertanian.* 17(1), 27-35.

[4] Khairunisa. R. (2008). Kombinasi Teknik Elektrolisis Dan Teknik Adsorpsi Menggunakan Karbon Aktif Untuk Menurunkan Konsentrasi Senyawa Fenol Dalam Air. *Skripsi*, FMIPA Universitas Indonesia.

[5] Rizna, S. R. (2017). Pemanfaatan Adsorben Alami (Biosorben) Untuk Mengurangi Kadar Timbal (Pb) Dalam Limbah Cair. *Prosiding Seminar Nasional Biotik 2017,* 271-279.

[6] Efendi, D. A. M. N., Ramandani, A. A., Cendekia, D., & Hanifah, W. (2023). Industrial wastewater treatment using venture injector type Micro-bubble aeration as a reduction of dissolved Iron (Fe2+) levels. *Journal of Natural Sciences and Mathematics Research,* 9(2).

[7] Sari, N. P., Dewi, A. I., Teguh, D., & Wulandari, Y. R. (2023). Pengaruh Konsentrasi Karbon Disulfida (Cs2) Terhadap Kinerja Biosorben Selulosa Xanthate Untuk Penjerapan Logam Berat. *Jurnal Sains dan Teknologi Lingkungan,* 15(2), 177-192.

[8] Hendra, D. (2006). The Manufacture of Activated Charcoal from Oil Palm Shells and Mixture of Wood Sawdust. *Penelitian Hasil Hutan,* 24(2), 1-22.

[9] Najmia, H., Mahreda, E. S., Mahyudin, R. P., & Kissinger. (2021). Pemanfaatan Arang Aktif Cangkang Kelapa Sawit Teraktivasi H3PO4 untuk Penurunan Kadar Besi (Fe), Mangan (Mn) dan Kondisi pH pada Air Asam Tambang. *Jurnal Enviro Scientea,* 17(2), 21-29.

[10] Hanum, F., Bani, O., & Wirani, L. (2017). Characterization of activated carbon from rice husk by HCl activation and its application for lead (Pb) removal in car battery wastewater. *IOP Conference Series: Materials Science and Engineering*, 180 (1).

[11] Kielbasa, K., Bayar, S., Varol, E. A., Srenscek-Nazzal, J., Boscaka, M., Miadlicki, P., Serafin, J., Wrobel, R. J., & Michalkiewicz, B. (2022). Carbon dioxide adsorption over activated

carbons produced from molasses using H2SO4, H3PO4, HCl, NaOH, and KOH as activating agents. *Molecules*, 27(21), 7467.

[12] Tani, D. (2015). The effect of activation time on the chemical structure and quality of activated carbon from coconut shell charcoal using ZnCl2 activator. *International Journal of Applied Chemistry*, 11(1), 73-83.

[13] Neethu, B., Bhowmick, G., & Ghangrekar, M. (2019). A novel proton exchange membrane developed from clay and activated carbon derived from coconut shell for application in microbial fuel cell. *Biochemical Engineering Journal*, 148, 170-177.

[14] Gurten, I. I., & Aktas, Z. (2020). Enhancing the performance of activated carbon based scalable supercapacitors by heat treatment. *Applied Surface Science*, 514, doi: 10.1016/j.apsusc.2020.145895.

[15] Pradeep, G. G., Sukumaran, K. P., George, G., Muhammad, F., & Mathew, N. (2016). Production and Characterization of Activated Carbon and Its Application in Water Purification. *International Research Journal of Engineering and Technology*, 443-447.

[16] Ramandani, A. A., Shintawati, S., Aji, S. P., & S. Sunarsi. (2022). Pemanfaatan Lignin Serai Wangi Sebagai Lignin Resorsinol Formaldehida (LRF) Menggunakan Ultrasonic Microwave-Assisted Extraction (UMAE). *CHEESA: Chemical Engineering Research Articles*, 5(1), 40-40, doi: 10.25273/cheesa.v5i1.10348.40-48.

[17] Haji, A. G., Pari, G., Nazar, M., & Habibati, H. (2013). Characterization of activated carbon produced from urban organic waste. *International Journal of Science and Engineering*, 5(2), doi: 10.12777/ijse.5.2.89-94.

[18] Haji, A. G., Pari, G., Habibati., Amirrudin., & Maulina. (2010). Kajian Mutu Hasil Pirolisis Cangkang Kelapa Sawit. *Jurnal Purifikasi*, 11(1), 77-86.

[19] Wulandari, Y. R., Silmi, F. F., Ermaya, D., Sari, N. P., & Teguh, D. (2023) Pengaruh Suhu Pirolisis Jerami Padi Terhadap Variabel Komposisi Produk Pirolisis Menggunakan Reaktor Batch. *Inovasi Teknik Kimia*, 8(3), 167-172.

[20] Diharyo., Salampak., Damanik, Z., & Gumiri, S. (2020). Pengaruh lama aktifasi dengan H3PO4 dan ukuran butir arang cangkang kelapa sawit terhadap ukuran pori dan luas permukaan butir arang aktif. *Prosiding Seminar Nasional Lingkungan Lahan Basah*, 5(1), 48-54.

[21] Hendra D., & Darmawan, S. (2007). Sifat Arang Aktif Dari Tempurung Kemiri. *Jurnal Penelitian Hasil Hutan*, 25(4), 291-302.

[22] Botahala, L. (2019). *Perbandingan Efektivitas Daya Adsorpsi Sekam Padi dan Cangkang Kemiri terhadap Logam Besi (Fe) pada Air Sumur Gali*. Sleman: Deepublish, CV. Budi Utama.

[23] Syamsudin, K. W. A. (2017). Sintesis dan Karakterisasi Karbon Aktif Tandan Pisang Dengan Aktivator H3PO4 10% untuk Adsorpsi Logam Pb (II) Dan Cr (VI) Dalam Larutan. *Repository Universitas Islam Indonesia*. 1-109. Retrieved from https://dspace.uii.ac.id/123456789/27730.

[24] Hartanto, S., & Ratnawati, R. (2010). Pembuatan karbon aktif dari tempurung kelapa sawit dengan metode aktivasi kimia. *Jurnal Sains Materi Indonesia*, 12(1), 12-16.

[25] Wiskandar, W., & Fuadi, N, A. (2022). Pengaruh aplikasi biochar cangkang kelapa sawit dan pupuk kompos terhadap kemantapan agregat tanah lahan bekas tambang batubara dan hasil kedelai. *Respository Universitas Jambi*. Retrieved from https://repository.unja.ac.id/id/eprint/33537.

[26] Prasetyo, Y., & Nasrudin, H. (2013). Penentuan Konsentrasi ZnCl2 pada Proses Pembuatan Karbon Aktif Tongkol Jagung dan Penurunan Konsentrasi Surfaktan Linier Alkyl Benzene Sulphonate (LAS). *UNESA Journal of Chemistry*, 2(3), 231-235.

Kampus 3 Universitas PGRI Madiun
Jl. Auri No 14-16 Kartoharjo Madiun
Email: cheesa@unipma.ac.id
http://e-journal.unipma.ac.id/index.php/cheesa